Neuroscience
Computational and Systems Biology

# Estradiol elicits distinct firing patterns in arcuate nucleus kisspeptin neurons of females through altering ion channel conductances

**Jian Qiu, Margaritis Voliotis, Martha A. Bosch, Xiao Feng Li, Larry S. Zweifel, Krasimira Tsaneva-Atanasova, Kevin T. O'Byrne, Oline K. Rønnekleiv, Martin J. Kelly**

Department of Chemical Physiology and Biochemistry, Oregon Health & Science U., Portland, OR 97239, USA • Department of Mathematics and Statistics, University of Exeter, Stocker Rd, Exeter, EX4 4PY, UK • Living Systems Institute, University of Exeter, Stocker Rd, Exeter, EX4 4PY, UK • Department of Women and Children's Health, School of Life Course and Population Sciences, King's College London, Guy's Campus, London SE1 1UL, UK • Department of Psychiatry and Behavioral Sciences, University of Washington, Seattle, WA 98195, USA • Depatment of Pharmacology, University of Washington, Seattle, WA 98195, USA • Division of Neuroscience, Oregon National Primate Research Center, Beaverton, OR 97006, USA

https://en.wikipedia.org/wiki/Open_access
Copyright information

**Reviewed Preprint**

Published from the original preprint after peer review and assessment by eLife.

About eLife's process

**Reviewed preprint version 1**
May 7, 2024 (this version)

**Posted to preprint server**
February 23, 2024

**Sent for peer review**
February 20, 2024

## Abstract

Hypothalamic kisspeptin (Kiss1) neurons are vital for pubertal development and reproduction. Arcuate nucleus Kiss1 (Kiss1$^{ARH}$) neurons are responsible for the pulsatile release of Gonadotropin-releasing Hormone (GnRH). In females, the behavior of Kiss1$^{ARH}$ neurons, expressing Kiss1, Neurokinin B (NKB), and Dynorphin (Dyn), varies throughout the ovarian cycle. Studies indicate that 17β-estradiol (E2) reduces peptide expression but increases *Vglut2* mRNA and glutamate neurotransmission in these neurons, suggesting a shift from peptidergic to glutamatergic signaling. To investigate this shift, we combined transcriptomics, electrophysiology, and mathematical modeling. Our results demonstrate that E2 treatment upregulates the mRNA expression of voltage-activated calcium channels, elevating the whole-cell calcium current and contributing to high-frequency firing. Additionally, E2 treatment decreased the mRNA levels of Canonical Transient Receptor Potential (TPRC) 5 and G protein-coupled $K^+$ (GIRK) channels. When TRPC5 channels in Kiss1$^{ARH}$ neurons were deleted using CRISPR, the slow excitatory postsynaptic potential (sEPSP) was eliminated. Mathematical modeling confirmed the importance of TRPC5 channels for initiating and sustaining synchronous firing, while GIRK channels, activated by Dyn binding to kappa opioid receptors, were responsible for repolarization. Our findings suggest that E2 modifies ionic conductance in Kiss1$^{ARH}$ neurons, enabling the transition from high frequency synchronous firing through NKB-driven activation of TRPC5 channels to a short bursting mode facilitating glutamate release. In a low E2 milieu, synchronous firing of Kiss1$^{ARH}$ neurons drives pulsatile release of GnRH, while the transition to burst firing with high, preovulatory levels of E2 facilitates the GnRH surge through its glutamatergic synaptic connection to preoptic Kiss1 neurons.

**eLife assessment**

This study addresses the effects of estrogen on the kisspeptin1 subset of neurons in the arcuate nucleus of the hypothalamus of female mice after ovaries were surgically removed. The authors repeat some of their prior work and provide new and interesting findings about the effects of estrogen on currents mediated by calcium and potassium channels, suggest a neurotransmitter "switch", and suggest Trpc5 regulates Kisspeptin 1 neuron excitability. While **useful** in its significance, there are concerns that the evidence for some conclusions is **incomplete**. This study will be of interest to endocrinologists and reproductive biologists.

# Introduction

Hypothalamic kisspeptin (Kiss1) neurons and its cognate receptor (GPR 54 or Kiss1 R) are essential for pubertal development and reproduction, and may also be involved in the control of energy homeostasis (Kotani et al., 2001) (De Roux et al., 2003) (Seminara et al., 2003) (Messager et al., 2005) (Shahab et al., 2005) (d'Anglemont de Tassigny et al., 2008) (Qiu J. et al., 2018) (Rønnekleiv et al., 2022). Kisspeptin neurons within the arcuate nucleus of the hypothalamus ($Kiss1^{ARH}$) co-express Kiss1, Neurokinin B (NKB) and Dynorphin (Dyn), which are all down-regulated by 17β-estradiol (E2) (Goodman et al., 2007; Navarro V. M. et al., 2009). However, $Kiss1^{ARH}$ neurons also express vesicular glutamate transporter 2 (vGlut2) and release glutamate, and both vGlut2 expression and glutamate release are upregulated by E2 in females (Qiu J. et al., 2018). This indicates that peptides and glutamate in $Kiss1^{ARH}$ neurons are differently modulated by E2 and suggests that there is a complex E2 regulation in these neurons such that they transition from predominantly peptidergic to glutamatergic neurotransmission and hence from a "pulsatile" to "surge" mode (**Figure 1**). It has been known for decades that neurons located within the arcuate nucleus are responsible for the pulsatile release of GnRH and subsequently pulsatile release of LH from the pituitary gland (O'Byrne et al., 1991) (Moenter et al., 1993). In this respect, it is now generally accepted that $Kiss1^{ARH}$ neurons are the main neurons responsible for the generation of pulsatile LH release, but the underlying cellular conductances generating this activity have not been elucidated.

Morphological studies have provided evidence that $Kiss1^{ARH}$ neurons can communicate directly with each other (Lehman et al., 2010) (Navarro V. M. et al., 2009) (Navarro V.M. et al., 2011). Furthermore, $Kiss1^{ARH}$ neurons express the NKB receptor, Tacr3, as well as the kappa (κ) opioid receptor (KOR), whereas GPR54 is not expressed in $Kiss1^{ARH}$ neurons, rendering them unresponsive to kisspeptin (d'Anglemont de Tassigny et al., 2008; Navarro V. M. et al., 2009; Wakabayashi et al., 2010). Using optogenetics and whole-cell recordings we demonstrated that high-frequency photoactivation of $Kiss1^{ARH}$ neurons induces a NKB-mediated slow excitatory postsynaptic potential (EPSP), which is mediated by the recruitment of canonical transient receptor potential (TRCP5) channels. The release of NKB is limited by co-released dynorphin, which acts presynaptically to inhibit further release. Together the two peptides cause synchronized firing of $Kiss1^{ARH}$ neurons (Kelly et al., 2018; Qiu J. et al., 2016; Qiu Jian et al., 2021), whereas kisspeptin and glutamate appear to be the main output signals from $Kiss1^{ARH}$ neurons (Qiu J. et al., 2016; Qiu J. et al., 2018) (Voliotis et al., 2021) (Liu et al., 2021).

Although single action potential-generated calcium influx is sufficient to trigger the release of classical neurotransmitters such as glutamate, high frequency (10-20 Hz) is required for the release of neuropeptides such as kisspeptin, NKB and dynorphin (Qiu J. et al., 2016). Indeed, the slow EPSP, which underlies the synchronization, is similar to the "plateau potential" that has been

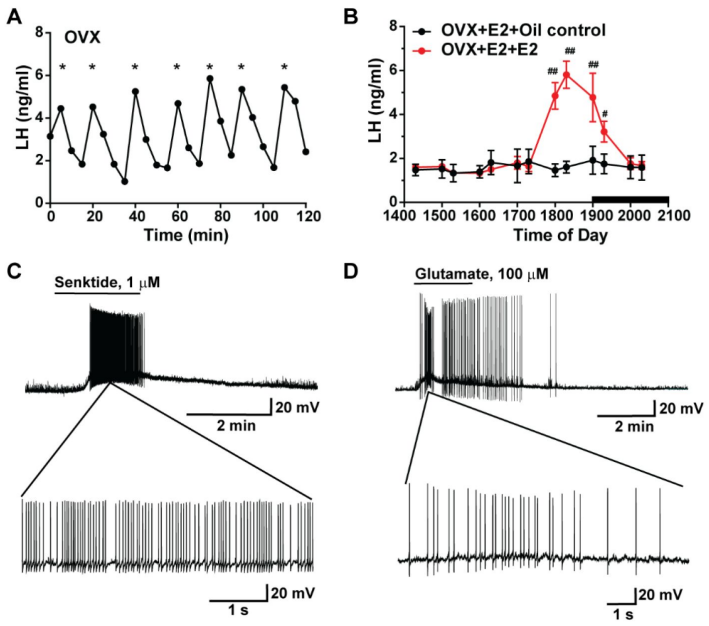


## Figure 1.

### LH pulse and surge profiles in mice with associated firing activity of Kiss1$^{ARH}$ neurons.

**A**, Representative example of an LH pulse profile in an ovariectomized (OVX) mouse in the absence of gonadal steroid feedback. Pulses detected by the DynPeak algorithm are indicated with an asterisk (Lin et al., 2021). **B**, LH surge profile (closed symbol) in mice undergoing the OVX+E2+E2 surge inducing protocol (6-10 days post OVX and implantation of 17β-estradiol capsule delivering diestrous levels of steroid, mice received subcutaneous injections of estradiol benzoate (1μg/20g body weight) on 2 consecutive days at 08:30 h with blood samples collected every 30 min from 14:30 - 20:30 h for LH measurement (Lin et al., 2021); mean ± SEM; (n=9). Open symbol representing control mice not receiving the second dose of estradiol benzoate (OVX+E2+oil). The expected LH surge occurred approximately 1 h before lights off (19:00 h). Values significantly different from basal LH concentrations are indicated by # ($^{\#}p<0.05$, $^{\#\#}p<0.01$, repeated measures ANOVA). **C**, illustration of synchronized firing of a Kiss1$^{ARH}$ neuron induced by TACR3 agonist senktide in an OVX female. **D**, demonstration of burst firing of a Kiss1$^{ARH}$ neuron induced by glutamate in an E2-treated, OVX female. The spike activities in C and D have been expanded to emphasize the notable effects of senktide or glutamate on the firing activity of Kiss1$^{ARH}$ neurons.

described in hippocampal and cortical neurons (Arboit et al., 2020; Zhang Z. et al., 2011). Many neurons, including Kiss1$^{ARH}$ neurons, express the biophysical properties that allow them to continue to persistently fire even after a triggering synaptic event has subsided (Zylberberg and Strowbridge, 2017) (Qiu J. et al., 2016). Moreover, the intrinsic bi-stability of neurons that generates persistent firing activity has been linked to a calcium-activated, non-selective cation current ($I_{CAN}$) (Zylberberg and Strowbridge, 2017), and TRPC channels, specifically TRPC5 channels, are thought to be responsible for the $I_{CAN}$ in cortical neurons (Zhang Z. et al., 2011). Therefore, we postulate that TacR3 activation via NKB drives influx of $Ca^{+2}$ through TRPC5 channels leading to greater build-up of $[Ca^{2+}]_i$ that facilitates the opening of more TRPC5 channels in a self-sustaining manner. Indeed, using the fast intracellular calcium chelator BAPTA, which has been shown to robustly inhibit TRPC5 channel activation in heterologous cells (Blair et al., 2009), we have been able to abolish the slow EPSP and persistent firing in Kiss1$^{ARH}$ neurons following optogenetic stimulation in female mice (Qiu Jian et al., 2021).

Although the expression of peptides in Kiss1$^{ARH}$ neurons are downregulated by high circulating levels (late follicular levels) of E2, the intrinsic excitability of and the glutamate release by Kiss1$^{ARH}$ neurons are increased by *Cacna1g* (Cav3.1, T-type calcium channel), *Hcn1* and *Hcn2* (Hyperpolarization-activated, Cyclic Nucleotide Gated channels) mRNA expression and Vglut2 mRNA expression, respectively (Qiu J. et al., 2018). Burst firing in CNS neurons, which efficiently releases fast amino acid transmitters like glutamate, is generated primarily by the T-type calcium channel current ($I_T$) (*e.g.*, in thalamic relay neurons), and the rhythmicity of this burst firing is dependent on the h-current ($I_h$) (for review, see (Lüthi and McCormick, 1998; Zagotta and Siegelbaum, 1996)). $I_h$ is mediated by the HCN channel family, which includes channel subtypes 1-4, of which *Hcn1* and *Hcn2* are the main channels in Kiss1$^{ARH}$ neurons. $I_h$ depolarizes neurons from hyperpolarized states, raising the membrane potential into the range of $I_T$ activation (Erickson et al., 1993a, 1993b; Kelly and Rønnekleiv, 1994; Lüthi and McCormick, 1998; Zhang C. et al., 2009). $I_T$ is mediated by the low-threshold voltage-gated calcium channels, $Ca_V$3.1-3.3 (for review see (Perez-Reyes, 2003)). $I_T$ initiates a transient $Ca^{2+}$-driven depolarization above the threshold for action potential initiation (*i.e.*, a low threshold spike) (Llinás, 1988; Tsien et al., 1987). This depolarization then drives neurons to fire an ensemble (burst) of $Na^+$-driven action potentials.

Based on the above compelling evidence we postulated that Kiss1$^{ARH}$ neurons transition from peptidergic neurotransmission, driving the pulsatile release of GnRH via kisspeptin release into the median eminence, to glutamatergic transmission that facilitates in the preovulatory surge of GnRH (Lin et al., 2021) through their projection to the Kiss1$^{AVPV}$ neurons (Qiu J. et al., 2016). Therefore, we initiated studies to thoroughly characterize effects of high circulating (late follicular) levels of E2 on the expression of the full complement of voltage-activated calcium channels (and currents) and the opposing $K^+$ channels, involved in the repolarization, on the excitability of Kiss1$^{ARH}$ neurons. We performed whole-cell recordings and single cell RT-PCR analysis of Kiss1$^{ARH}$ neurons to determine which channels are involved in the physiological transition from peptidergic to glutamatergic neurotransmission. Our physiological findings were incorporated into a mathematical model that accounts for the E2 effects on the firing activity of Kiss1$^{ARH}$ neurons and validates our hypothesis that high levels of E2 facilitate the transition from peptidergic to glutamatergic neurotransmission.

# Results

## Whole-cell current of voltage-activated $Ca^{2+}$ channels in $Kiss1^{ARH}$ neurons

Previously, we have shown that an increase in the intracellular calcium concentration can potentiate TRPC5 channel current in POMC neurons (Qiu J. et al., 2010). Additionally, chelating intracellular calcium with BAPTA abolishes the slow excitatory postsynaptic potential (EPSP) and persistent firing in $Kiss1^{ARH}$ neurons (Qiu Jian et al., 2021). Here, to investigate the contributions of voltage-activated calcium channels (VGCCs) to the increase in intracellular calcium, we measured the peak calcium current contributed by both the low and high voltage-activated calcium channels. To assess VGCC activity, we employed 150-ms test pulses starting from a holding potential of -80 mV with 10-mV increments, ultimately reaching a test potential of +40 mV in $Kiss1^{ARH}$ neurons. The inward currents evoked by the voltage pulses were identified as calcium ($Ca^{2+}$) currents, as they were blocked by the universal VGCC inhibitor $Cd^{2+}$ (200 μM) (McNally et al., 2020) (**Figures 2A-E**). The maximum total inward and $Cd^{2+}$-sensitive currents reached their peak amplitudes at -10 mV. To differentiate between various calcium channel subtypes present in $Kiss1^{ARH}$ neurons, we applied selective antagonists individually, allowing us to isolate the drug-sensitive current for each cell. When we individually applied specific antagonists, we observed partial inhibition of the $Ca^{2+}$ currents. Treatment with 10 μM nifedipine (Hiraizumi et al., 2008; Kato et al., 2003; Lee et al., 2002), an L-type $Ca^{2+}$ channel inhibitor, resulted in a partial inhibition (26.0%) of the whole-cell calcium current. Additionally, application of 1 μM ω-conotoxin MVIIC (ConoMVIIC, targeting N/P/Q-type channels) (Nunemaker et al., 2003), 2 μM ω-conotoxin GVIA (conoGVIA, targeting N-type channels) (Lee et al., 2002), 200 nM ω-agatoxin IVA (AgaIVA, targeting P/Q-type channels) (Kato et al., 2003; McNally et al., 2020), 100 nM SNX-482 (targeting R-type channels) (Hiraizumi et al., 2008), or 1 μM TTA-P2 (TTAP2, targeting T-type channels) (McNally et al., 2020) also led to partial inhibition of the $Ca^{2+}$ currents (**Figure 2F**). The observed reduction in current with each inhibitor indicates the presence of all the major subtypes of $Ca^{2+}$ currents in $Kiss1^{ARH}$ neurons. Among the inhibitors used, the largest components of the whole-cell calcium current was found to be sensitive to nifedipine (26.1%), conoGVIA (25.1%), and SNX-482 (31.1%) (**Figures 2A, B, D and 2F**). Subsequently, we documented contributions from TTA-P2-sensitive channels, accounting for approximately 6.7% of the total $Ca^{2+}$ current, and AgaIVA-sensitive channels, which constituted approximately 3.9% (**Figures 2E, C**). These findings indicate that high voltage-activated L-, N-, and R-type channels constitute the largest components of the voltage-activated $Ca^{2+}$ current in $Kiss1^{ARH}$ neurons that not only increase the overall excitability but also greatly facilitate TRPC5 channel opening (Blair et al., 2009), which is the major downstream target of TACR3 activation by NKB (Qiu J. et al., 2016).

## Voltage-activated $Ca^{2+}$ channels contribute to generation of slow-EPSP in $Kiss1^{ARH}$ neurons

Our previous study utilizing optogenetics demonstrated that high-frequency photostimulation of $Kiss1^{ARH}$ neurons releases NKB. This release of NKB induces slow excitatory postsynaptic potentials (EPSPs) and facilitates the recruitment of other $Kiss1^{ARH}$ neurons, resulting in synchronous firing of the $Kiss1^{ARH}$ neuronal population (Qiu J. et al., 2016). Additionally, chelating intracellular calcium with the fast chelator BAPTA abolishes the slow EPSP and persistent firing in $Kiss1^{ARH}$ neurons, highlighting the role of calcium signaling in these processes (Qiu Jian et al., 2021). To access the involvement of HVA channels in the generation of the slow EPSP, we conducted experiments where we blocked the L-type $Ca^{2+}$ channels with nifedipine (10 μM) and the N- and P/Q-type $Ca^{2+}$ channels with ω-conotoxin MVIIC (1 μM). We then measured the

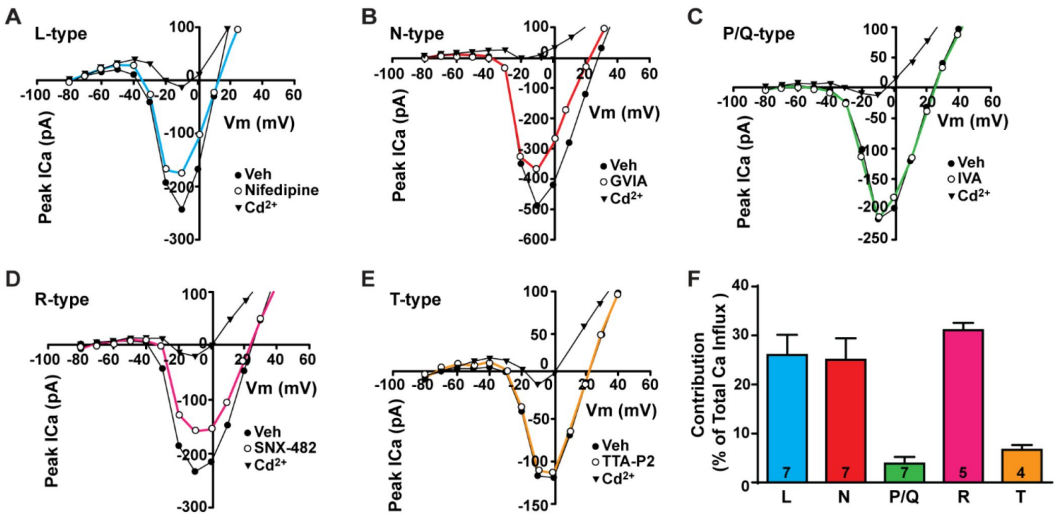


## Figure 2.

### Relative contribution of voltage-gated calcium currents in *Kiss1*$^{ARH}$ neurons from OVX mice.

**A-E**, representative current –voltage relationships showing that $Cd^{2+}$ (non-selective blocker of calcium channels) sensitive peak currents were inhibited by different calcium channel blockers: A, nifedipine; B, ω-conotoxin GIVA; C, ω-agatoxin IVA; D, SNX-482; E, TTA-P2. **F**, the maximum peak currents were measured at -10 mV. The proportions of $Ca^{2+}$ currents inhibited by nifidipine (L type), ω-conotoxin GVIA (N type), ω-agatoxin IVA (P/Q), SNX-482 (R type) and TTA-P2 (T type). Data are expressed as mean ± SEM, n = cell numbers.

slow EPSP. Indeed, both nifedipine and ω-conotoxin MVIIC significantly inhibited the slow EPSP by 42.9% and 60.4%, respectively (**Figure 3**). In addition, we used SNX (100 nM), which selectively blocks R-type $Ca^{2+}$ channels, and the slow EPSP was reduced to 28.7% of its control value (**Figure 3C**). The selective T-channel blocker TTA-P2 (5 μM) inhibited the slow EPSP by 28.6% (*data not shown*). Therefore, it appears that all of the calcium channels contribute to maintaining the sustained depolarization underlying the slow EPSP.

## E2 increases the mRNA expression and the whole-cell current of voltage-activated $Ca^{2+}$ channels

The neuropeptides NKB (tachykinin2, *Tac2*) and kisspeptin (*Kiss1*), which are expressed in $Kiss1^{ARH}$ neurons, are crucial for the pulsatile release of gonadotropin-releasing hormone (GnRH) and reproductive processes. E2 decreases the expression of *Kiss1* and *Tac2* mRNA in $Kiss1^{ARH}$ neurons but enhances the excitability of $Kiss1^{ARH}$ neurons by amplifying the expression of *Cacna1g*, *Hcn1*, and *Hcn2* mRNA, as well as increasing T-type calcium currents and h-currents (Qiu, 2018, 20613}. Moreover, E2 drives Slc17a6 mRNA expression and enhances glutamatergic synaptic input to arcuate neurons and $Kiss1^{AVPV}$ neurons (Qiu J. et al., 2018). As a result, the E2-driven increase in $Kiss1^{ARH}$ neuronal excitability and glutamate neurotransmission may play a crucial role in triggering the surge of GnRH, ultimately leading to the LH surge.

To assess the impact of E2 on the modulation of voltage-activated calcium channels and $Kiss1^{ARH}$ neuronal excitability, we employed real-time PCR (qPCR) to measure the relative expression levels of ion channel subtypes in $Kiss1^{ARH}$ neurons. We compared the expression in E2-treated females to those treated with oil, using the specific primers listed in **Table 1**. The quantification was conducted on pools of 5 or 10 neurons, as indicated in the Methods. In both oil- and E2-treated females, we quantified the expression of *Cav1.2* (L-type), *Cav2.1* (P/Q-type), *Cav2.2* (N-type) and *Cav2.3* (R-type) mRNAs. Remarkably, all of these mRNA transcripts exhibited increased expression levels in response to E2 treatment (**Figure 4A and B**). Congruent with our previous findings (Qiu J. et al., 2018), we observed that the mRNA expression of *Cav3.1*, *Hcn1*, and *Hcn2* was also upregulated in response to E2 treatment (**Figure 4C**). These results suggested that E2 has a regulatory effect on the expression and function of all of these ion channels in $Kiss1^{ARH}$ neurons. To determine whether the increased mRNA expression translated into functional changes at the cellular level, we measured the whole-cell calcium current in $Kiss1^{ARH}$ neurons obtained from ovariectomized mice treated with either vehicle or E2. We discovered that E2 treatment led to a significant increase in the peak calcium current density in $Kiss1^{ARH}$ neurons, which was recapitulated as predicted by our computational modeling (**Figure 5A-D**). These findings indicate that the upregulation of the mRNA expression of calcium channels by E2 translated to an augmented peak calcium current in $Kiss1^{ARH}$ neurons.

The largest components of the calcium currents in $Kiss1^{ARH}$ neurons from the E2-treated, ovariectomized females were found to be sensitive to nifedipine, conoGVIA, and SNX-482, accounting for approximately 24.9%, 24.6%, and 27.0% of the total current across cells, respectively, which is very similar to their contributions to the whole-cell current from vehicle-treated, ovariectomized females (**Figure 3**). In addition, contributions from TTA-P2-sensitive channels accounted for approximately 11.1% of the total $Ca^{2+}$ current, while agaIVA-sensitive channels contributed to approximately 11.0% (**Figure 5E**). These results highlight the prevalence of L-, N-, and R-type calcium channels as the major contributors to the whole-cell calcium current in $Kiss1^{ARH}$ neurons from E2-treated, ovariectomized females, but also the involvement of T-type and P/Q-type channels.

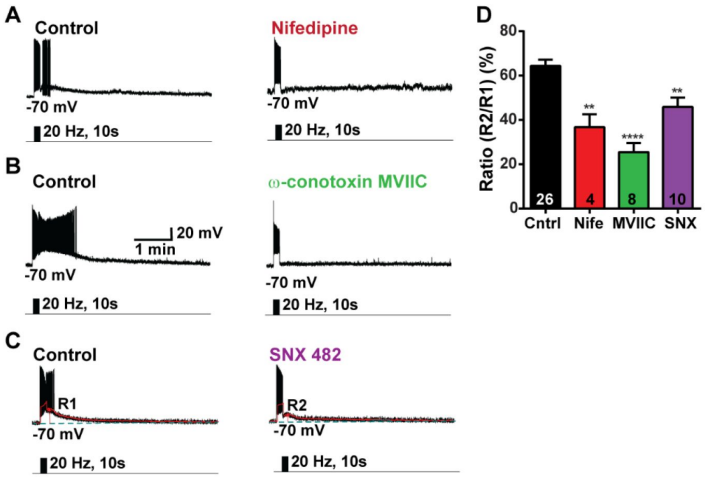


## Figure 3.

### Blockade of HVA $Ca^{2+}$ channels decreases the slow EPSP in *Kiss1*$^{ARH}$ neurons.

**A-C**, representative traces showing that the slow EPSPs were abolished by perfusing the blocker of the L-type calcium channel, nifedipine (A) or N- and P/Q -type calcium channels, ω-conotoxin MVIIC (B), or the R-type calcium channel, SNX 482 (C), respectively. The arrows indicate the measurements of slow EPSP amplitude, denoted as R1 and R2, after low-pass filtering. **D**. Bar graphs summarizing the effects of drugs on the R2/R1 ratios. The slow EPSP was generated in OVX Kiss1-Cre::Ai32 mice. Comparisons between different treatments were performed using a one-way ANOVA analysis ($F_{(3, 44)} = 19.72$, $p<0.0001$) with the Bonferroni's *post hoc* test. **, **** indicates $p<0.01$, 0.001, respectively vs. control.

| Gene Name (encodes for) | Accession Number | Primer Location (bp) | Product Length (bp) | Annealing Temp (°C) | Efficiency Slope | $r^2$ | % |
|---|---|---|---|---|---|---|---|
| *Cacna1c* (Cav 1.2 L-type) | NM_009781 | 1331-1348<br>1390-1407 | 77 | 60 | -3.478 | 0.989 | 94 |
| *Cacna1a* (Cav 2.1 P/Q-type) | NM_007578 | 6035-6054<br>6090-6109 | 75 | 60 | -3.498 | 0.980 | 93 |
| *Cacna1b* (Cav 2.2 (N-type) | NM_001042528 | 5405-5426<br>5467-5488 | 84 | 60 | -3.483 | 0.992 | 94 |
| *Cacna1e* (Cav 2.3 R-type) | NM_009782 | 530-549<br>617-636 | 107 | 60 | -3.441 | 0.983 | 95 |
| *Cacna1g* (Cav 3.1 T-type)[a] | NM_009783 | 5004-5025<br>5060-5083 | 80 | 60 | -3.372 | 0.968 | 98 |
| *Hcn1* (HCN1)[a] | NM_010408 | 1527-1546<br>1641-1662 | 136 | 60 | -3.253 | 0.958 | 100 |
| *Hcn2* (HCN2)[a] | NM_008226 | 1122-1143<br>1199-1218 | 97 | 60 | -3.279 | 0.969 | 100 |
| *Trpc5* (TRPC5) | NM_009428 | 734-753<br>832-851 | 118 | 60 | -3.161 | 0.952 | 100 |
| *Slc17a6* (vGluT2)[a] | NM_080853 | 872-889<br>967-984 | 113 | 60 | -3.293 | 0.920 | 100 |
| *Gapdh* (GAPDH)[a] | NM_008084 | 689-706<br>764-781 | 93 | 60 | -3.352 | 0.998 | 99 |
| *Kcnma1* (BK) | NM_001253358 | 2745-2762<br>2833-2852 | 108 | 60 | -3.338 | 0.971 | 99 |
| *Kcnn3* (SK3) | NM_080466 | 1259-1277<br>1352-1370 | 112 | 60 | -3.369 | 0.952 | 98 |
| *Kcnj6* (GIRK2) | NM_001025584 | 488-507<br>592-609 | 122 | 60 | -3.368 | 0.919 | 98 |
| *Kcnq2* (KCNQ2) | NM_010611 | 1079-1098<br>1151-1170 | 92 | 60 | -3.367 | 0.978 | 98 |
| *Kcnb1* (KCNB1) | NM_008420 | 691-710<br>759-780 | 119 | 60 | -3.375 | 0.983 | 98 |
| *Kcnd2* (KCND2) | NM_019697 | 2135-2156<br>2217-2238 | 104 | 60 | -3.312 | 0.972 | 100 |

[a] primers published in (Qiu J. et al., 2018)

**Table 1.**

**Primer Table**

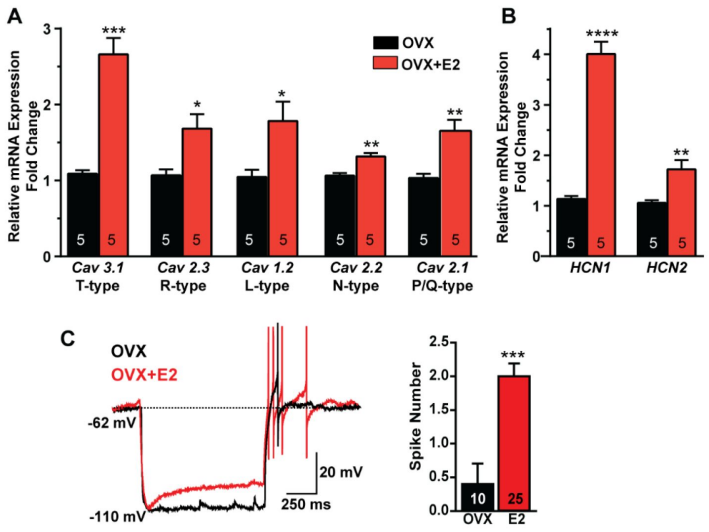


## Figure 4.

### A, E2 increases the expression of low and high voltage-activated calcium channels in Kiss1$^{ARH}$ neurons.

Kiss1$^{ARH}$ neurons (three to four 10-cell pools) were harvested from each of 5 vehicle- and 5 E2-treated, OVX females to quantify ion channel mRNA expression of low and high voltage activated calcium channels as described in the Methods. The analysis included: T-type (Cav3.1) low voltage-activated, as well as the following high-voltage activated channels: R-type (Cav 2.3), L-type (Cav 1.2), N-type (Cav 2.2) and P/Q-type (Cav 2.1) calcium channels. Interestingly, all of these channels were upregulated with E2 treatment, which significantly increased the whole-cell calcium current (see Figure 5). **B**, E2 also increased the expression of hyperpolarization-activated, cyclic-nucleotide gated HCN1 and HCN2 channels in Kiss1$^{ARH}$ neurons. The same Kiss1$^{ARH}$ neuronal pools were also analyzed for mRNA expression of HCN1 and HCN2 ion channels. HCN1 channel mRNA expression was the most highly upregulated by E2 treatment in Kiss1$^{ARH}$ neurons; although, the mRNA expression of HCN2 was also significantly increased. The expression values were calculated via the ΔΔCT method, normalized to GAPDH and relative to the oil control values. Bar graphs represent the mean ± SEM. * $p < 0.05$, ** $p < 0.01$, *** $p < 0.005$, **** $p < 0.001$, oil versus E2. **C**, in addition, we have shown previously that E2-treatment also increases the associated T- and h-currents (not shown), as well as the neuronal excitability (measured as rebound excitation) in Kiss1$^{ARH}$ neurons. The left panel illustrates an example of rebound burst firing in Kiss1$^{ARH}$ neurons, while the right panel displays bar graphs representing the mean ± SEM. *** $p < 0.005$ (Qiu J. et al., 2018).

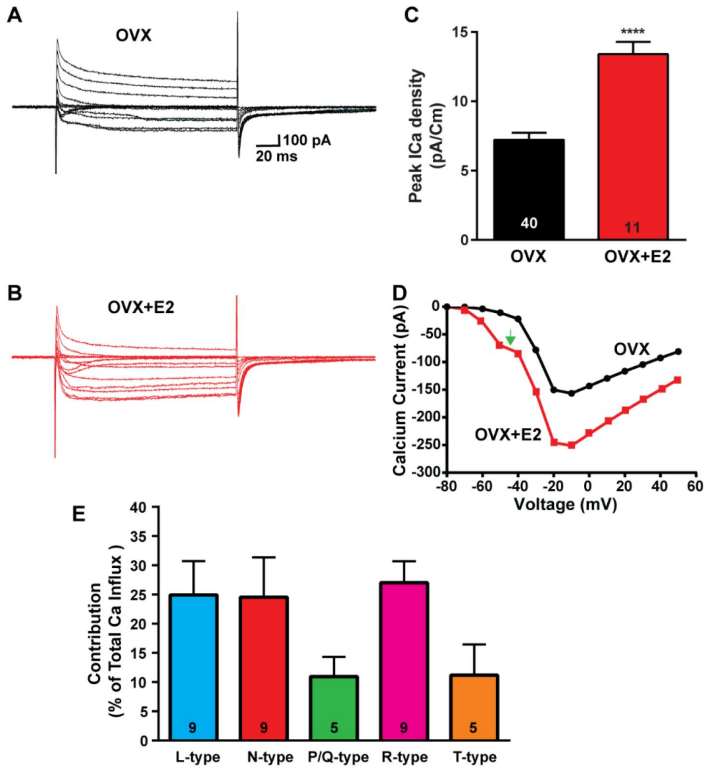


**Figure 5.**

### E2 treatment (positive-feedback regimen) increases the $Ca^{2+}$ currents in *Kiss1*$^{ARH}$ neurons.

**A-B**, $Ca^{2+}$ currents in *Kiss1*$^{ARH}$ neurons with the same membrane capacitance from oil-treated (A) or E2-treated (B) animals. **C**, the maximum peak currents were measured at -10 mV. The current amplitudes were normalized to the cell capacitance in all cases to calculate current density. The bar graphs summarized the density of $Ca^{2+}$ current in *Kiss1*$^{ARH}$ neurons from oil-treated and E2-treated animals. The mean density was significantly greater in E2-treated (13.4 ± 0.9 pA/pF, n = 11) than in oil-treated OVX females (7.2 ± 0.5 pA/pF, n = 40) (unpaired two-tailed t-test, $t_{(49)} = 5.75$, ****$p < 0.0001$). **D**. The modeling predicts that E2-treated, OVX females exhibit a significantly greater inward $Ca^{2+}$ current (red trace) than the vehicle-treated females (black trace). The green arrow in the red trace indicates the T-channel "inflection." **E**. Relative contribution of voltage-gated calcium currents in *Kiss1*$^{ARH}$ neurons from OVX, E2-treated mice. The maximum peak currents were measured at -10 mV. The proportions of $Ca^{2+}$ currents inhibited by nifidipine (L type), ω-Conotoxin GVIA (N type), ω-agatoxin IVA (P/Q), SNX-482 (R type) and TTA-P2 (T type). Data are expressed as mean ± SEM, n = cell numbers.

## E2 does not alter the kinetics of calcium channel activation or de-inactivation

In order to determine whether the increase in peak voltage-activated calcium current density was the result of E2 regulating calcium channel kinetics, mRNA expression or both, we examined the voltage dependence of activation and inactivation. By measuring the voltage dependence of activation, we assessed how E2 affects the ability of calcium channels to open in response to membrane potential changes. Similarly, by examining the voltage dependence of inactivation, we determined how E2 influences the inactivation kinetics of calcium channels. Based on our results, there was no difference in the voltage dependence of activation between cells from the vehicle-treated control group ($V_{1/2}$ = -32.3 ± 2.1 mV; n = 13) and cells from estrogen-treated females ($V_{1/2}$ = -33.6 ± 2.5 mV; n = 11). Similarly, there was not a significant difference in the voltage dependence of inactivation between control cells ($V_{1/2}$ = -48.9 ± 4.8 mV; n = 6) and estrogen-treated cells ($V_{1/2}$ = -44.1 ± 1.9 mV; n = 5) (**Figure 6**). Therefore, although E2 increased the mRNA expression of HVA calcium channels, it did not affect the channel kinetics in $Kiss1^{ARH}$ neurons. Furthermore, our previous studies established that there is no difference in the voltage dependence of activation and inactivation of T-type calcium channels in hypothalamic arcuate neurons between the vehicle-treated and E2-treated, ovariectomized females (Qiu J. et al., 2006). Also, E2 downregulated the expression of *Kcnd2* mRNA encoding Kv4.2, which is expressed in $Kiss1^{ARH}$ neurons (Mendonça et al., 2018) and has similar kinetics of activation as the T-type calcium channels (Oil-treated, ovariectomized females relative mRNA expression: 1.053, n = 5 animals versus E2-treated expression: 0.5643, n=5; t-test p = 0.0061). This opposing $K^+$ current would dampen the inward calcium current. Therefore, it appears that E2 does not modulate calcium channel kinetics directly but rather alters the mRNA expression to increase the conductance.

## BK, SK and KCNQ channels are involved in modulating excitability of $Kiss1^{ARH}$ neurons

In the brain, calcium plays a crucial role in sculpting neuronal firing by activating potassium channels, which subsequently influence neuronal behavior (Nicoll, 1988; Storm, 1990). Since HVA and LVA calcium channels were expressed in $Kiss1^{ARH}$ neurons, all of which contribute to the elevation of intracellular calcium concentration ($[Ca^{2+}]_i$) that facilitates TRPC5 channel opening (Blair et al., 2009), our next step involved measuring the changes in $Ca^{2+}$-activated $K^+$ channel conductances and assessing their mRNA expression. In various cell types increases in cytosolic calcium levels, whether resulting from extracellular influx or intracellular release, lead to the activation of plasma membrane calcium-dependent potassium channels (Sah Pankaj and Louise Faber, 2002). Similarly, in $Kiss1^{ARH}$ neurons, these channels would be activated by calcium influx through all four types of high voltage-gated calcium channels, as well as the low voltage-activated calcium channel, which are all active during action potential firing. The activity of $Ca^{2+}$-activated $K^+$ channels play a crucial role in numerous physiological processes, including secretion and the regulation of neuronal firing properties. Two main families of $Ca^{2+}$-activated $K^+$ channel channels have been characterized, distinguished by their biophysical and pharmacological properties. These families are known as BK (Big Conductance $K^+$) and SK (Small Conductance $K^+$) channels in the CNS (Kshatri et al., 2018). BK channels are known for their high potassium selectivity and large single channel conductance, typically ranging from 100 to 300 pS. Activation of BK channels requires both calcium binding and membrane depolarization (Blatz and Magleby, 1987; Marty, 1989; Sah P., 1996; Storm, 1990). On the other hand, SK channels are simply activated by increases in cytosolic calcium levels, with their half-maximal activation at 0.3 μM (Bond et al., 1999).

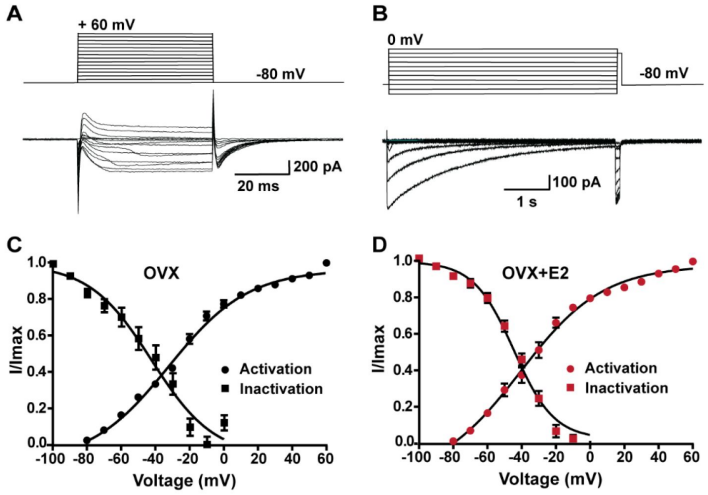


**Figure 6.**

**Voltage dependence of $I_{Ca}$ in *Kiss1*$^{ARH}$ neurons from OVX and OVX+E2 mice.**

**A-B**, top panels: activation and inactivation protocol. Bottom: representative traces. **C-D**, the mean $V_{1/2}$ values for calcium channel activation were not significantly different for cells from controls versus cells from estrogen-treated females. Similarly, the $V_{1/2}$ values for channel steady-state inactivation were similar for both groups.

To investigate $K^+$ currents, the cells were maintained at a holding potential of -70 mV while being exposed to blockers CNQX, AP5, picrotoxin and TTX. Subsequently, the membrane potential was stepped by depolarizing voltages, ranging from -60 mV to +40 mV in 10 mV increments, for a duration of 500 ms (Brereton et al., 2013). This protocol was employed to activate $K^+$ currents (**Figure 7A**). First, we examined SK currents. The mean current density was determined at the end of the voltage pulses. In vehicle-treated, OVX females the application of the SK channel blocker apamin (100 nM) (Spergel, 2007) led to a significant reduction in whole-cell currents in the +20 to +40 mV range (**Figures 7A, B**). The mean outward current density at +40 mV in the control group was 125.5 ± 13.1 pA/pF (n = 3) with the apamin-sensitive component contributing 56.2 ± 2.3 pA/pF (n = 3) (**Figures 7A, C**). In contrast, in the E2-treated females, the overall mean outward current density at +40 mV was 191.8 ± 17.4 pA/pF (n = 5), which was significantly greater than the vehicle control group (**Figures 7D, E**). However, there was no significant difference in the apamin-sensitive component between the vehicle-treated and E2-treated females, 56.2 ± 2.3 pA/pF versus 63.8 ± 5.5 pA/pF (n = 4), respectively (**Figure 7F**). Our computational model was calibrated so that SK channels contributed ~50 pA/pF to the whole-cell outward $K^+$ current in E2-treated females (**Figure 7H**).

Furthermore, to investigate the expression of the mRNAs encoding SK channel subunits in $Kiss1^{ARH}$ neurons from vehicle-treated and E2-treated OVX females, qPCR experiments were performed on 10-cell $Kiss1^{ARH}$ neuronal pools (**Figure 7G**). We focused on SK3 channels because these channels exhibit the highest expression in the hypothalamus and E2 regulates their expression (Bosch et al., 2002). E2 treatment had no effect on the mRNA expression of the *SK3* subunit. These findings support our electrophysiology results.

Additionally, following the same protocol and in the presence of the same cocktail of blockers (CNQX, AP5, picrotoxin and TTX), we investigated the contribution of BK channels to $Kiss1^{ARH}$ neuronal excitability. In the OVX females, the application of the BK channel blocker iberiotoxin (ibTx, 200 nM) (Niday and Bean, 2021) resulted in only a slight attenuation of the outward current (n = 5) (**Figures 8A, B**). The ibTx-sensitive current density measured at +40 mV was 31.1 ± 8.4 pA/pF (**Figures 8A, C**). However, in the E2-treated females, the application of ibTx significantly attenuated the whole-cell $K^+$ current from +30 to +40 mV, (**Figures 8D, E**). Additionally, the ibTx-sensitive current was significantly larger in the +0 to +40 mV range in the E2-treated females compared to the OVX females (**Figure 8F**). These findings indicate that E2 treatment modulates the activity of ibTx-sensitive BK current in $Kiss1^{ARH}$ neurons, resulting in increased current density (100.9 ± 11.7 pA/pF versus 31.1 ± 8.4 pA/pF at +40 mV). Hence our computational model was calibrated so that BK channels contributed ~100 pA/pF to the whole cell outward $K^+$ current in the E2-treated females (**Figures 8H**).

To investigate the expression of mRNA encoding BK channel subunits in $Kiss1^{ARH}$ neurons from vehicle-treated and E2-treated OVX females, qPCR experiments were performed on 10-cell $Kiss1^{ARH}$ neuronal pools (**Figure 8G**). E2 treatment significantly increased the mRNA expression of the BKα1 (*Kcnma1*) subunit. These findings support our electrophysiological findings that there is a significant increase in BK channel activity in $Kiss1^{ARH}$ neurons with E2 treatment (**Figure 8F**). In addition, E2 increased the mRNA expression of *Kcnb1* encoding Kv2.1 (E2-treated relative mRNA expression: 1.672, n = 5 versus oil-treated mRNA expression: 1.086, n = 5; t-test p-value = 0.0024). The combination of the up-regulation of the two of these $K^+$ channels would facilitate rapid repolarization of $Kiss1^{ARH}$ following an action potential.

Traditionally, the after hyperpolarization is divided into three distinct phases: fast (fAHP), medium (mAHP), and slow after hyperpolarization (sAHP) (Storm, 1990; Vogalis et al., 2003). The fast after hyperpolarization (fAHP) is primarily mediated by the BK family of potassium channels (Storm, 1987). The medium after hyperpolarization (mAHP) is predominantly mediated by apamin-sensitive SK2 channels (Bond et al., 2004; Peters et al., 2005). However, KCNQ family members contribute to both the mAHP and sAHP (Tzingounis A. V. et al., 2010; Tzingounis A. V.

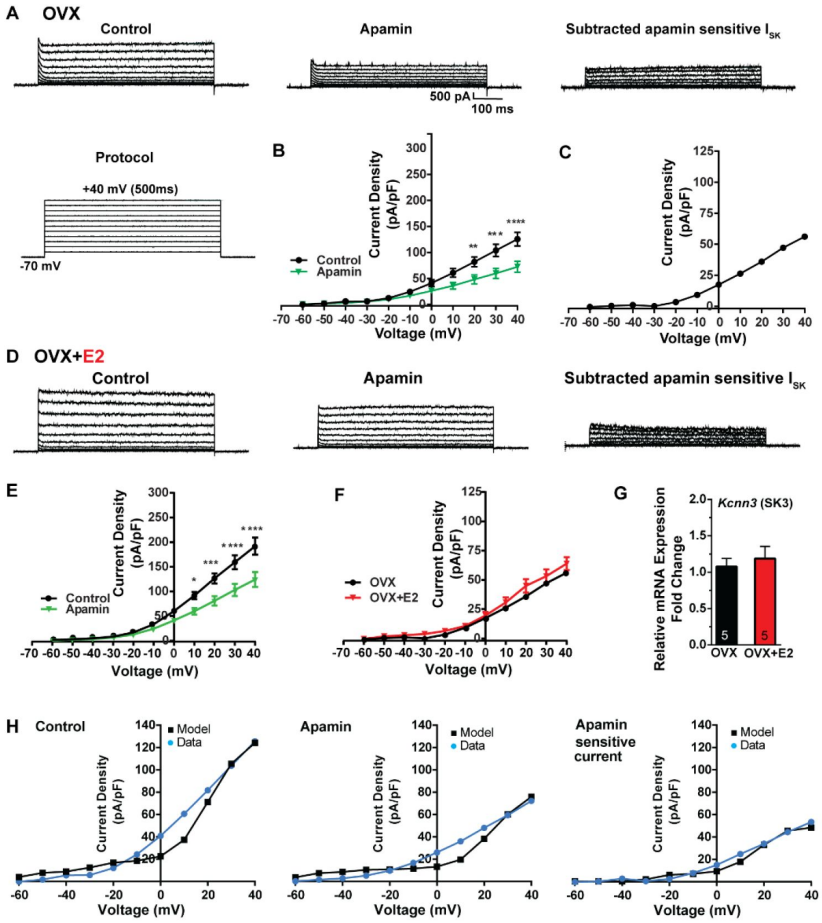


## Figure 7.

### Small conductance, calcium-activated $K^+$ (SK) channel is involved in repolarization of burst firing *Kiss1*$^{ARH}$ neurons in OVX and E2-treated, OVX mice.

**A**. Representative traces of the inhibition of outward currents before (left, control) and after the specific SK blocker Apamin (500 nM, middle). Apamin sensitive currents were calculated from the subtraction of control and apamin at depolarized potentials (right). Cells were clamped at -70 mV and given 500 ms voltage pulses from - 60 mV to +40 mV in 10 mV steps at 0.2 Hz, as shown in A at the bottom. **B**. Mean current density-voltage relationships measured at the end of the 500 ms voltage step ranging from -60 mV to +40 mV were obtained in the absence and presence of apamin (two-way ANOVA: main effect of treatment ($F_{(1, 4)}$ = 7.697, p = 0.0501), main effect of time ($F_{(10, 40)}$ = 99.3, p < 0.0001) and interaction ($F_{(10, 40)}$ = 7.645, p < 0.0001); mean ± SEM; n = 3; *post hoc* Bonferroni test, **p < 0.01, ***p < 0.005, ****p < 0.001). **C**. Apamin sensitive current densities were obtained from C (mean ± SEM, n = 3). **D**. Representative traces of the inhibition of outward currents before (left, control) and after the specific SK blocker Apamin (500 nM, middle). Apamin sensitive currents were resulted from the subtraction of control and apamin at depolarized potentials (right). **E**. Mean current density-voltage relationships measured at the end of the 500 ms voltage step ranging from -60 mV to +40 mV were obtained in the absence and presence of apamin (two-way ANOVA: main effect of treatment ($F_{(1, 8)}$ = 9.433, p = 0.0153), main effect of time ($F_{(10, 80)}$ = 184.9, p < 0.0001) and interaction ($F_{(10, 80)}$ = 8.791, p < 0.0001); mean ± SEM, n = 4; *post hoc* Bonferroni test, *p < 0.05, ***p < 0.005, ****p < 0.001). **F**. Apamin sensitive current densities were obtained from C and E (ns; Two-way ANOVA followed by Bonferroni *post hoc* test; mean ± SEM; OVX, n = 3; OVX+E2, n = 4). **G**. Kiss1$^{ARH}$ neurons (three to four 10-cell pools) were harvested from each of 5 vehicle- and 5 E2-treated, OVX females to quantify the mRNA expression of SK3 ion channel. E2 did not increase the mRNA expression small conductance calcium-activated $K^+$ (SK3) channels in Kiss1$^{ARH}$. The expression values were calculated via the ΔΔCT method, normalized to GAPDH and relative to the oil control values. Bar graphs represent the mean ± SEM (unpaired two-tailed t-test for SK3, ns). **H**. The mathematical model was calibrated on the electrophysiology data from Kiss1$^{ARH}$ neurons for E2-treated females before and after treatment with the specific SK blocker apamin, left panel versus middle panel respectively (see Table S1 for $g_{SK}$). The modeled apamin-sensitive current (right panel) matches the electrophysiological data. For the calibration it was assumed that the applied concentration of apamin (500nM) completely blocked the SK current.

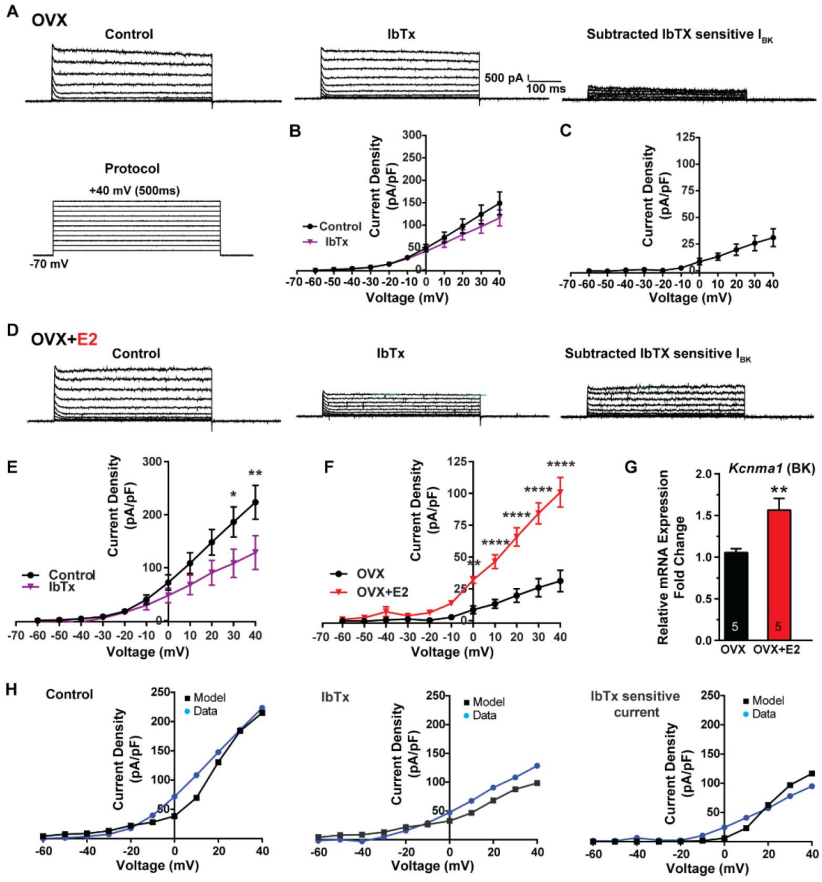


## Figure 8.

### Large conductance, calcium-activated $K^+$ (BK) channels contributes to the repolarization of $Kiss1^{ARH}$ neurons in OVX and E2-treated, OVX mice.

**A**. Representative traces of the inhibition of outward currents before (left, control) and after the specific BK blocker iberiotoxin (IbTx; 200 nM, middle). IbTx sensitive currents were calculated from the subtraction of control and IbTx at depolarized potentials (right). Cells were clamped at -70 mV and given 500 ms voltage pulses from -60 mV to +40 mV in 10 mV steps at 0.2 Hz, as shown in A at the bottom. **B**. Mean current density-voltage relationships measured at the end of the 500 ms voltage step ranging from -60 mV to +40 mV were obtained in the absence and presence of IbTx (two-way ANOVA: main effect of treatment ($F_{(1, 8)}$ = 0.8841, p = 0.3746), main effect of time ($F_{(10, 80)}$ = 71.56), p < 0.0001) and interaction ($F_{(10, 80)}$ = 1.127, p = 0.3528); mean ± SEM, n = 5; *post hoc* Bonferroni test, p > 0.05). **C**. IbTX sensitive current densities were obtained from B (mean ± SEM, n = 5). **D**. Representative traces of the inhibition of outward currents before (left,control) and after the specific BK blocker iberiotoxin (IbTx; 200 nM, middle). IbTx sensitive currents were resulted from the subtraction of control and IbTx at depolarized potentials (right). **E**. Mean current density-voltage relationships measured at the end of the 500 ms voltage step ranging from -60 mV to +40 mV were obtained in the absence and presence of IbTX (two-way ANOVA: main effect of treatment ($F_{(1, 6)}$ = 3.181, p = 0.1248), main effect of time ($F_{(10, 60)}$ = 52.90, p < 0.0001) and interaction ($F_{(10, 60)}$ = 3.667, p = 0.0007); mean ± SEM, n = 4; *post hoc* Bonferroni test, *p < 0.05, **p < 0.01). **F**. IbTx sensitive current densities were obtained from C and E (two-way ANOVA: main effect of treatment ($F_{(1, 7)}$ = 31.63, p = 0.0008), main effect of time ($F_{(10, 70)}$ = 80.41, p < 0.0001) and interaction ($F_{(10, 70)}$ = 21.54, p <0.0001); mean ± SEM, OVX, n = 5; OVX+E2, n = 4; Bonferroni *post hoc* test, **p < 0.01, ****p < 0.001). **G**. $Kiss1^{ARH}$ neurons (three to four 10-cell pools) were harvested from each of 5 vehicle- and 5 E2-treated, OVX females to quantify the mRNA expression of BKα channel. E2-treatment increased the mRNA expression of BKα. The expression values were calculated via the ΔΔCT method, normalized to GAPDH and relative to the oil control values. Bar graphs represent the mean ± SEM (unpaired two-tailed t-test for BK, $t_{(6)}$ = 3.479, **p < 0.01). **H**. The mathematical model was calibrated to reproduce the current voltage relationship observed in $Kiss1^{ARH}$ neurons from E2-treated animals (see Table S1 for $g_{BK}$) before and after treatment with IbTx. The modeled IbTx -sensitive current (right panel) matches the electrophysiological data. For the calibration it was assumed that the applied concentration of IbTx (200nM) completely blocked the BK current.

and Nicoll, 2008). Therefore, to investigate the contribution of KCNQ channels to Kiss1$^{ARH}$ neuronal excitability, voltage clamp experiments were conducted in the presence of TTX, CNQX, AP5, and picrotoxin, and a standard M-current protocol was run using the M-channel blocker XE-991 to isolate the M-current (Greene et al., 2017; Roepke et al., 2011) (**Figure 9 A, B**). The application of XE-991 resulted in the inhibition of M-current within a physiologically relevant voltage range of -60 to -30 mV in E2-treated OVX females but exhibited minimal impact in OVX females (**Figure 9 C, D**). Although the XE991-sensitive current was relatively small compared to other voltage-activated $K^+$ conductances, it demonstrated a significant increase in E2-treated, OVX females (**Figures 9 E**). The maximum peak current density sensitive to XE-991 at -30 mV was found to be four times higher in E2-treated OVX females when compared to OVX females. This would contribute to the repolarization following burst firing. Furthermore, E2 increased the mRNA expression of *Kcnq2*, (**Figure 9F**), which suggests that KCNQ channels play a key role in repolarizing Kiss1$^{ARH}$ neurons following burst firing. Indeed, our modeling predicted that M-current contributed to the repolarization following burst firing (**Figure 9G**).

## E2 increases Vglut2 but down regulates Tac2, Trpc5 and Girk2 mRNA expression in Kiss1$^{ARH}$ neurons

Based on our electrophysiological results, Kiss1$^{ARH}$ neurons appear to transition from peptidergic to glutamatergic neurotransmission through E2-mediated changes in the expression of voltage-activated $Ca^{2+}$ channels and $K^+$ channels, and their respective conductances. Therefore, we asked the question is there a difference in peptide and glutamate mRNA expression mediating this transition? Therefore, we ran a comparison between *Tac 2* (NKB) and *Vglut2* (surrogate for glutamate) expression. The cycle threshold (CT) was compared between *Tac2* and *Vglut2* as well as *Kiss1*, *TRPC5* and *GIRK2* in Kiss neuronal cell pools from OVX oil-treated and OVX E2-treated animals (**Figures 10A, B**). It is worth noting that lower number of cycles illustrate a higher quantity of mRNA expression because the fluorescence is detected earlier, and one cycle difference represents a doubling in expression. As expected, the reference gene *Gapdh* did not change with E2-treatment. However, quantitative PCR results revealed that E2 treatment of OVX females significantly reduced *Tac2* expression (**Figure 10C**), whereas *Vglut2* mRNA was significantly increased in Kiss1$^{ARH}$ neurons (**Figure 10D**). Moreover, both *Trpc5* and *Girk2* expression were significantly reduced in E2-treated, OVX females (**Figures 10E, F**).

## CRISPR mutagenesis of Trpc5 attenuates slow EPSP and reduces excitability of Kiss1$^{ARH}$ neurons

Our computational modeling suggested that TRPC5 channels play a dominant role in regulating cell excitability. Therefore, as proof of principle, we utilized a CRISPR approach to mutate TRPC5 channels in Kiss1$^{ARH}$ neurons similar to our previous studies (Hunker et al., 2020; Stincic et al., 2021). Hunker *et al.* developed a single viral vector for conditional expression of the smaller *Staphylococcus aureus* (SaCas9) and sgRNA that yields high-efficiency mutagenesis in specific cell types (Hunker et al., 2020). To selectively mutate *Trpc5* in Kiss1$^{ARH}$ neurons, we generated two guide RNA's, one targeting exon 2, which is conserved across all splice variants, and the other targeting exon 7, the pore forming domain (**Figures 11A, B**). A cohort of Kiss1$^{ARH}$ mice were given bilateral stereotaxic injections into the ARH of the two AAV1-FLEX-SaCas9-sgTrpc5's or a control virus containing the Trpc5 guide with three base pairs in the seed region mutated (SaCas9-control) as described (Hunker et al., 2020). An additional Cre-dependent virus of the same serotype (AAV1) that drove expression of a fluorophore (YFP or mCherry) was co-administered in order to visualize injection quality and facilitate harvesting of cells (**Figure 11C**). After three weeks, mice underwent ovariectomy since OVX mice express the maximum slow EPSP amplitude (Qiu J. et al., 2016). Brain slices were prepared, and cells harvested as previously described (Qiu J. et al., 2018) and analyzed with qPCR. We found that the *Trpc5* mutagenesis group displayed a

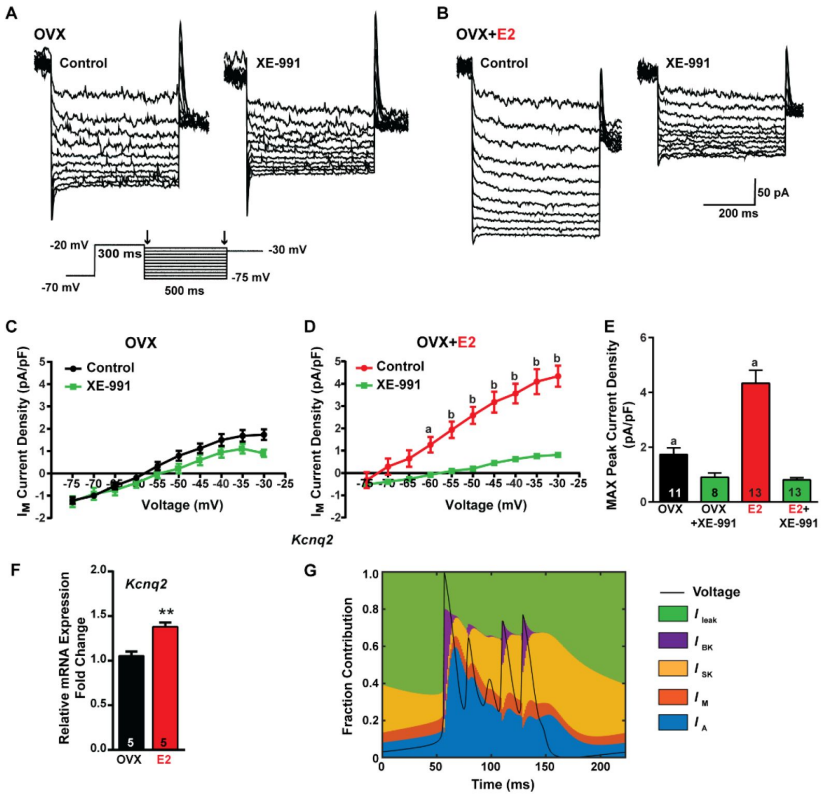


## Figure 9.

### KCNQ channels (M-current) contribute to the slow AHP in *Kiss1*$^{ARH}$ neurons.

**A**-**B**. Representative current traces of the M-current inhibition caused by 40 μM XE-991 perfused for 10 min in (A) OVX-oil and (B) OVX+E2-treated female mice. Inset: M-current deactivation protocol. **C**-**D**. Current density-voltage plots from –75 to –30 mV of vehicle and XE-991 perfusion in (C) OVX-oil and (D) OVX+E2-treated mice. Two-way ANOVA for C: main effect of treatment ($F_{(1, 17)}$ = 1.908, p = 0.1851), main effect of time ($F_{(9, 153)}$ = 187.1, p < 0.0001), and interaction ($F_{(9, 153)}$ = 3.901, p = 0.0002); Veh, n = 11; XE-991, n = 8; Bonferroni *post hoc* test, p > 0.05. For D: main effect of Veh and XE-991 ($F_{(1, 24)}$ = 24.92, p < 0.0001), main effect of time ($F_{(9, 216)}$ = 174.5, p < 0.0001), and interaction ($F_{(9, 216)}$ = 52.75, p < 0.0001); Veh, n = 13; XE-991, n = 13; Bonferroni *post hoc* test, a = p < 0.05, b = p < 0.001. **E**. Treatment with E2 elevated, while XE-991 diminished the maximum peak current density elicited by a -30 mV step in OVX- and OVX+E2-treated mice. Two-way ANOVA: main effect of Veh and XE-991 ($F_{(1, 41)}$ = 47.59, p < 0.0001), main effect of OVX and OVX+E2 ($F_{(1, 41)}$ = 15.76, p = 0.0003), and interaction ($F_{(1, 41)}$ = 18.2, p = 0.0001; Veh, n = 11; XE-991, n = 8; Bonferroni *post hoc* test, Veh: OVX vs. OVX+E2, a = p < 0.001. XE-991: OVX vs. OVX+E2, p > 0.05. **F**. Kiss1$^{ARH}$ neurons (three to four 10-cell pools) were harvested from each of 5 vehicle- and 5 E2-treated, OVX females to quantify the mRNA expression of *Kcnq2*. E2 treatment increased the mRNA expression of *Kcnq2*. Unpaired t-test, $t_{(8)}$ = 4.850, **p = 0.0013. **G**. Percent contribution of the different $K^+$ currents to the repolarization current during burst-type firing activity in the OVX+E2 state. At each time point, the length of each color bar denotes the percent contribution of the corresponding current to the total outward current.

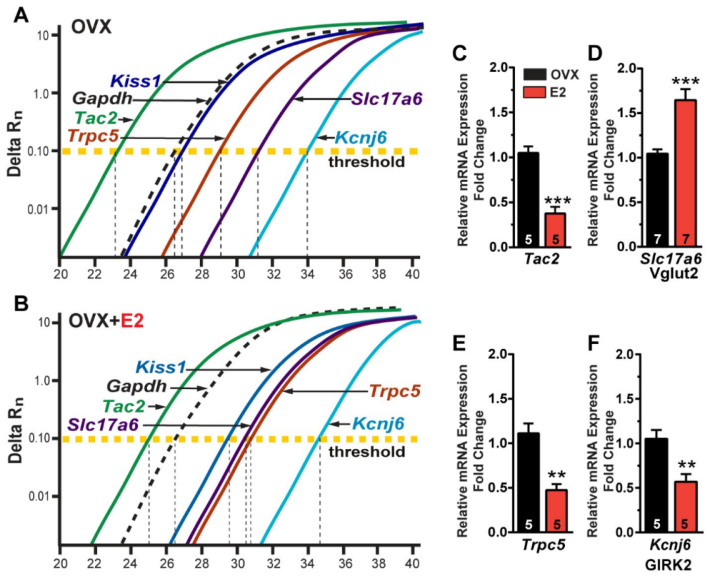


**Figure 10.**

## Estradiol decreases *Tac 2, Trpc5 and Kcnj6* but increases *Vglut 2* mRNA expression in Kiss1$^{ARH}$ neurons.

**A**. qPCR amplification curves illustrating the cycle threshold (CT) for *Tac2, Gapdh, Kiss1, Trpc5, Slc17a6 (Vglut2) and Kcnj6* (*GIRK2)* in Kiss1$^{ARH}$ five cell (C,D,E) or ten cell (F) neuronal pools (three to six pools from each animal) in OVX Oil-treated, and **B**, in OVX E2-treated females. **C**. Quantitative real-time PCR analysis of *Tac2* mRNA (n=5 animals), **D**, *Vglut2* (n=7 animals), **E**, *Trpc5* (n=5 animals), **F**, *Kcnj6* (n=5 animals). Comparisons were made between Oil-treated and E2-treated, OVX females using the comparative $2^{-\Delta\Delta CT}$ method. Bar graphs represent the mean ± SEM (Unpaired t test for *Tac2*, $t_{(6)}$= 6.350, p<0.001; Unpaired t test for *Vglut2*, $t_{(8)}$= 4.522, p<0.001; Unpaired t test for *Trpc5*, $t_{(6)}$= 4.818, p<0.01; Unpaired t test *for Kcnj6*, $t_{(6)}$= 3.457, p<0.01). The data for C and D (*Tac2* and *Slc17a6*) has been published previously (Qiu J. et al., 2018 ).

reduction in relative expression of *Trpc5* in Kiss1$^{ARH}$ neurons compared to the control group (**Figure 11D**). Hence, the qPCR data verified that in the *sgTrpc5*-targeted mice we can selectively reduce *Trpc5* gene expression in targeted cells.

As predicted, mutagenesis of Trpc5 in Kiss1$^{ARH}$ neurons significantly attenuated the slow EPSP (**Figures 12A, B, C**) such that the postsynaptic excitation was reduced to a "trickle" of action potential firing. What we would not have predicted is that the double sgRNA mutagenesis of *Trpc5* channels in Kiss1$^{ARH}$ neurons significantly hyperpolarized the resting membrane potential by 7 mV (**Figure 12D**). Moreover, the rheobase (minimum current required to induce firing) significantly increased by ~20% in females bearing the *sgTrpc5* double mutagenesis (**Figure 12E**). The firing frequency versus injected current (F-I) curve for sg*Trpc5* double mutagenesis Kiss1$^{ARH}$ neurons was also significantly attenuated (**Figure 12F**). In agreement with these experimental findings, simulations of our mathematical model confirmed that TPRC5 channels should lower the rheobase and greatly enhance the firing activity of Kiss1$^{ARH}$ neurons (**Figures 12G, H**). Finally, we employed our mathematical model to further investigate the transition from synchronous firing driven by NKB release and TRPC5 channel activation to burst firing generated by E2-mediated upregulation of endogenous conductances. Our simulations suggest that synchronous firing is indeed sculpted by the interplay between TRPC5 and GIRK channels, whereas burst firing is controlled by the E2-dependent increase of calcium and calcium-activated $K^+$ conductances (**Figure 13**).

# Discussion

We have shown that E2 plays a critical role in transitioning the glutamatergic/peptidergic Kiss1$^{ARH}$ neurons from a high frequency firing mode for synchronization, which is dependent on NKB-driven activation of TRPC5 channels, to a short bursting mode that would facilitate glutamate release. E2 decreased the expression of the peptide neurotransmitters NKB (kisspeptin and dynorphin) and TRPC5 channels but increased the mRNA expression of *Vglut2* and voltage-activated calcium channels that contribute to burst firing and glutamate release from the Kiss1$^{ARH}$ neurons. We determined that the increase in mRNA expression of the HVA calcium channels translated into a significant increase in whole-cell current with all of the calcium channels contributing proportionally. Most importantly the kinetics of activation and inactivation were unaltered with E2 treatment, which indicates that other post-translation modifications were not affecting channel activity. Surprisingly and somewhat counter intuitive, the *BK α1* subunit was also upregulated, but based on our modeling the rapid repolarization of the Kiss1$^{ARH}$ neurons (*i.e.*, the fast AHP) facilitates higher frequency of action potential firing. Moreover, our modeling confirmed that TRPC5 channels, which generate the slow EPSP (*a.k.a.*, plateau potential in other CNS neurons), are vital for initiating and sustaining synchronous firing of Kiss1$^{ARH}$ neurons, while concurrent activation of GIRK channels repolarizes Kiss1$^{ARH}$ neurons. E2 treatment of ovariectomized females decreased both *Trpc5* and *Girk2* channel mRNA expression, which in our model correlated with the reduction in sustained high frequency firing of Kiss1$^{ARH}$ neurons. Therefore, the synchronous high frequency firing of Kiss1$^{ARH}$ neurons in a low E2 milieu correlates with the pulsatile release of GnRH (LH from the pituitary gland), whereas the transition to burst firing in the presence of high circulating levels of E2 (*e.g.*, proestrus) facilitates the GnRH (LH) surge through its glutamatergic synaptic connection with Kiss1$^{AVPV/PeN}$ neurons.

## Core calcium conductances underlying synchronous and burst firing of Kiss1$^{ARH}$ neurons

TRPC5 channels are highly expressed in Kiss1$^{ARH}$ neurons (**Figure 11**), and TRPC5 channels are essentially ligand-activated calcium channels with a high permeability to calcium ($P_{Ca}/P_{Na}$ = 9:1) (Venkatachalam and Montell, 2007). In general, mammalian TRPC channels are activated by

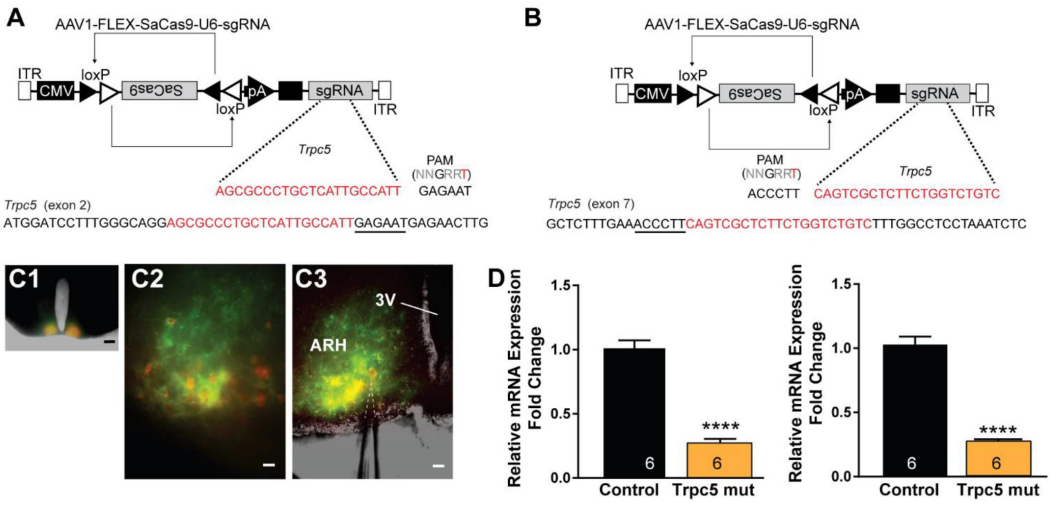


**Figure 11.**

### CRISPR mutagenesis of *Trpc5* channels in Kiss1$^{ARH}$ neurons.

**A**, structure of AAV1-FLEX-SaCas9-U6sg*Trpc5-exon2*. Exon 2 of *Trpc5* is denoted with guide sequence highlighted in red, the PAM is underlined. **B**. Structure of AAV1-FLEX-SaCas9-U6sg*Trpc5-exon7*. Exon 7 of *Trpc5* is denoted with guide sequence highlighted in red, the PAM is underlined. **C1**, image of coronal section through the ARH from Kiss1-Cre::Ai32 mouse with dual co-injections of AAV-DIO-mCherry and AAV1-FLEX-SaCas9-U6-sg*Trpc5*. Scale = 200 µm. **C2, C3**, higher power overlays of epifluorescence (EYFP & mCherry) images with recording pipette patched onto Kiss1$^{ARH}$-Cre:mCherry cell (C3). Scale = 40 µm. **D**, quantitative PCR measurements of *Trpc5* transcripts in double sgRNA mutagenesis of *Trpc5* (second sgRNA against pore forming region) in Kiss1$^{ARH}$ neurons. Primers were targeted to 1$^{st}$ or 2nd guide, respectively.

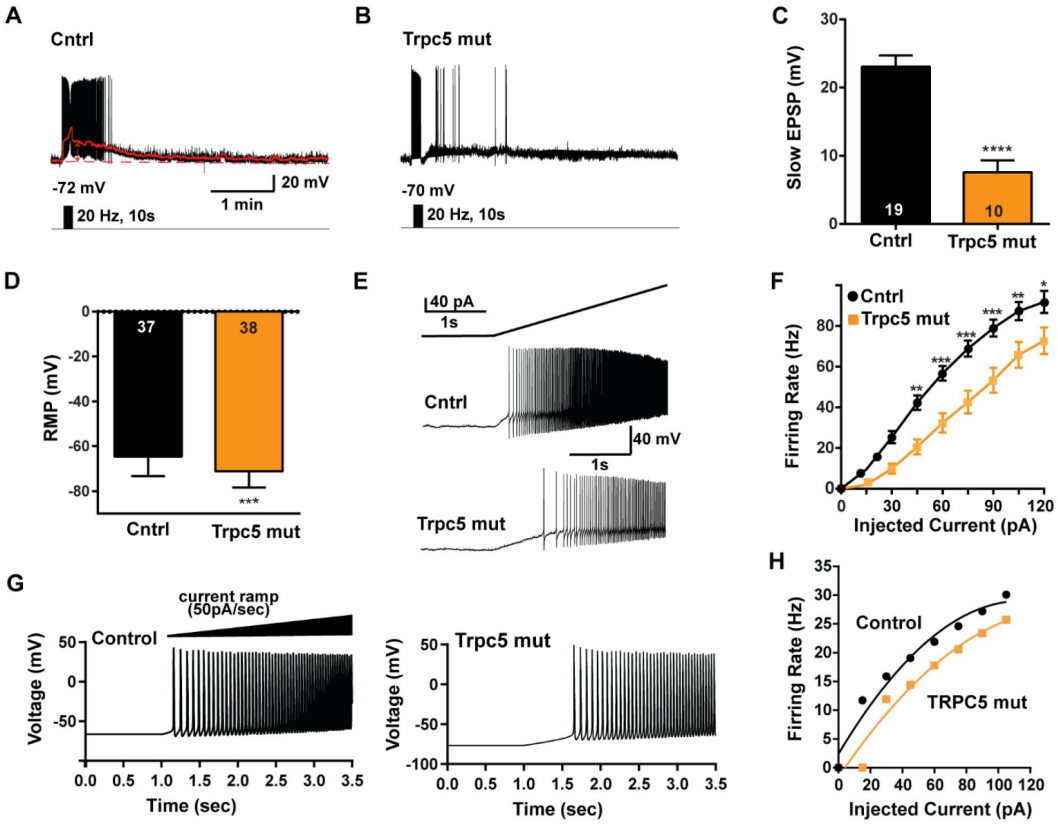


**Figure 12.**

**Double CRISPR mutagenesis of *Trpc5 attenuates slow EPSP*, increases rheobase and shifts the F-I curve.**

**A**, high-frequency photo-stimulation (20 Hz) generated slow EPSP in Kiss1$^{ARH}$ neuron from ovariectomized, control mouse. Red trace is slow EPSP after low-pass filtering. **B**, slow EPSP in Kiss1$^{ARH}$ neuron from OVX, double sg*Trpc5* -targeted mouse. **C**, summary of the effects of *Trpc5* mutagenesis on slow EPSP amplitude in female mice (**** $p < 0.0001$). **D**, double sgRNA mutagenesis of *Trpc5* channels in Kiss1$^{ARH}$ neurons significantly increased the RMP (control: -64.5±1.4 mV versus double sg*Trpc5* 1, 2: -71.1±1.2 mV, *$p = 0.0007$). **E**, current ramp showing the increased rheobase in sgTrpc5 double mutagenesis (control: 31.1±1.2 pA, n=31, versus sg*Trpc5* 1&2, 35.3±1.0 pA, n=33, $p = 0.0073$). **F**, firing frequency vs. current (F-I) curves for control versus sg*Trpc5* double mutagenesis (*<0.05; **<0.01 and ***$p < 0.005$, respectively). **G**, model simulations of the effects of a current ramp (50 pA/sec) for OVX (left panel) and OVX female with reduced (muted) TRPC5 conductance (right panel), and **H**, the associated firing frequency vs. current curves. In the latter case the TRCP5 conductance was halved, which is a conservative estimation of the CRISPR state in which the *Trpc5* is much more mutated in Kiss1$^{ARH}$ neurons (Figure 11).

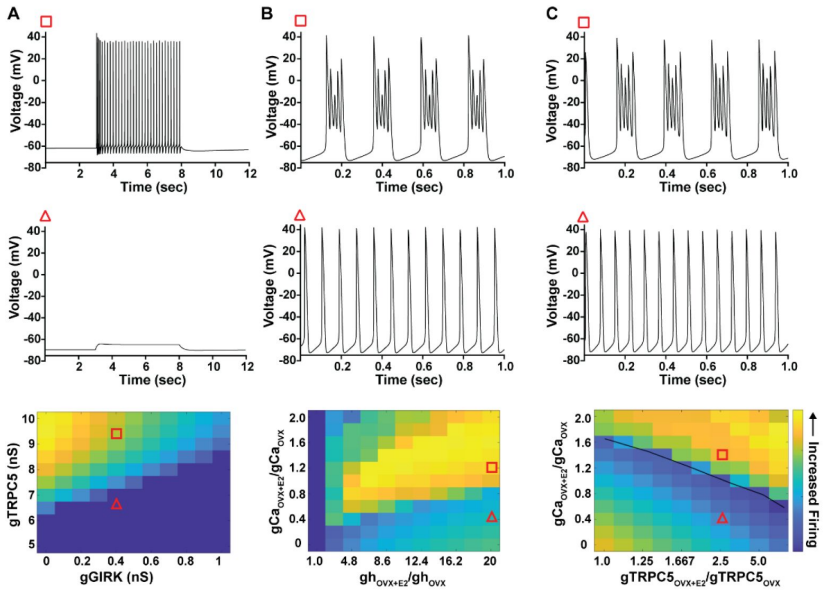


**Figure 13.**

### Computational modeling of a Kiss1$^{ARH}$ neuron in the OVX and OVX + E2 state demonstrates its distinct dynamic responses.

A model of the Kiss1$^{ARH}$ neuron was developed and calibrated using molecular data and electrophysiological recordings of Kiss1$^{ARH}$ neurons from OVX and OVX+E2 mice. **A**. Simulations of the OVX-parameterized model demonstrating high frequency activity in response to NKB stimulation. The balance between GIRK and TRCP5 conductance controls the response of the neuron to NKB stimulation, with neuronal response eliminated when TRPC5 conductance is low (red triangle) relative to the GIRK conductance. **B**. The OVX+E2 parameterized models demonstrate sustained burst firing activity. The bursting activity that is supported by elevated h- and Ca $^{2+}$-currents (red square). **C**. In the OVX+E2 state, burst firing activity is also supported by high conductance of HVA $Ca^{2+}$ channels relative to the conductance of TRPC5 channels. Representative points in the parameter space giving rise to burst firing activity are marked with red squares, whereas red triangles are used for points resulting in regular spiking. The black line separates these two regions of activity.

both G protein-coupled receptors and receptor tyrosine kinases (Ambudkar and Ong, 2007; Clapham, 2003), and are one of the major downstream effectors activated by glutamate binding to group I metabotropic glutamate receptors (mGluR1 and mGluR5) in CNS neurons (Bengtson et al., 2004; Berg et al., 2007; Faber et al., 2006; Tozzi et al., 2003). In substantia nigra dopamine neurons mGluR1 agonists induce a current that exhibits the tell-tale double-rectifying current-voltage plot of TRPC channel activation (Tozzi et al., 2003), similar to what we see with the effects of the NKB agonist senktide in $Kiss1^{ARH}$ neurons (Qiu Jian et al., 2021). Both mGluR1 and TacR3 are Gq-coupled to phospholipase C (PLC) activation which leads to hydrolysis of phosphatidylinositol 4,5-bisphosphate ($PIP_2$) to diacylglycerol (DAG) and inositol 1,4,5 triphosphate ($IP_3$), which is involved in channel activation (Birnbaumer, 2009). TacR3 (NKB) signaling has additional consequences since many $K^+$ (e.g., GIRK, KCNQ) channels are dependent on PIP2 for channel opening, and depletion of PIP2 by PLC leads to channel closure (Brown and Passmore, 2009) (Zhang C. et al., 2013) (Whorton and MacKinnon, 2011) (Zheng et al., 2022). Therefore, depletion of PIP2 by NKB signaling would further facilitate the sustained firing of $Kiss1^{ARH}$ neurons during synchronization.

A plateau potential has been characterized in hippocampal and cortical neurons (Arboit et al., 2020; Zhang Z. et al., 2011) as such these neurons express biophysical properties that allow them to continue to persistently fire even after a triggering synaptic event has subsided (Zylberberg and Strowbridge, 2017). The persistent firing activity of these neurons is linked to $I_{CAN}$ (Zylberberg and Strowbridge, 2017), and TRPC5 channels appear to be responsible for the $I_{CAN}$ (Zhang Z. et al., 2011). With TacR3 activation in $Kiss1^{ARH}$ neurons there is an influx of $Ca^{+2}$ through TRPC5 channels leading to greater build-up of $[Ca^{2+}]_i$ that facilitates the opening of more TRPC5 channels in a self-sustaining (autocatalytic) manner (Qiu J. et al., 2016). Using the fast intracellular calcium chelator BAPTA, which has been shown to robustly inhibit TRPC5 channel activation in heterologous cells (Blair et al., 2009), we abolished the slow EPSP and persistent firing of $Kiss1^{ARH}$ neurons following optogenetic stimulation (Qiu Jian et al., 2021). Moreover, HVA calcium channel blockers attenuated the generation of the slow EPSP (**Figure 3**) so it appears that they also contribute to the $I_{CAN}$ since calcium influx via both LVA and HVA calcium channels can also facilitate TRPC5 channel opening in $Kiss1^{ARH}$ neurons. In the ovariectomized female, treatment with E2 upregulated *Cav1.2, Cav2.1, Cav2.2, and Cav2.3 mRNA by 1.5-to 2-fold and Cav3.1* mRNA expression by ~3-fold. Hence, E2 significantly increased whole-cell calcium currents $Kiss1^{ARH}$ neurons, which greatly enhanced the excitability and contributed to the burst firing of $Kiss1^{ARH}$ neurons (present findings and (Qiu J. et al., 2018)). However, the amplitude of the slow EPSP with E2 treatment is only ~25% of the amplitude in the ovariectomized state (Qiu J. et al., 2016). Therefore, there appears to be a physiologic transition of $Kiss1^{ARH}$ neurons from the slow EPSP firing mode in the OVX state to the burst firing mode in the presence of E2, which has important physiologic ramifications as discussed below.

## TRPC5 and GIRK channels are vital for synchronization of $Kiss1^{ARH}$ neurons

Recently, Tian *et al.* demonstrated that TRPC4, a close homolog of TRPC5 sharing ~64 percent homology, is a “coincidence detector” of neurotransmission by both Gq/11 and Gi/o-coupled receptors in lateral septal (LS) neurons (Tian et al., 2022). In whole-cell recordings of LS neurons, TRPC 4 channels mediate a strong depolarizing plateau potential that in contrast to TRPC5 channel activation in $Kiss1^{ARH}$ neurons, abrogates action potential firing as a result of a depolarization block. In many instances the plateau potential in LS neurons is followed by an AHP, which is dependent on the activation of Gi/o-coupled receptors. In contrast, we have not observed an AHP in $Kiss1^{ARH}$ neurons following the slow EPSP (Qiu J. et al., 2016). Tian and colleagues showed that the depolarizing plateau in LS neurons is codependent on activation of both Gq/11-coupled mGluR1 glutamate receptors and Gi/o-coupled γ-aminobutyric acid type B receptors, the latter activating GIRK channels. Moreover, the firing patterns in LS neurons encodes information about the relative strengths of these contrasting inputs (*i.e.*, Gq/11 versus Gi/o) such that only

mGluR1 produces weak depolarization accompanied by increased firing of LS neurons, whereas pure $GABA_B$ receptor activation hyperpolarizes the cells and abrogates firing activity. Coincident input of both mGluR1 and $GABA_B$ receptors results in a brief burst of action potentials followed by a pause in firing, and both the pause duration and firing recovery patterns reflect the relative strengths of Gq/11 versus Gi/o inputs. Importantly, Tian and colleagues computationally simulated these various scenarios with computational modeling, and similar to our modeling, utilized only TRPC4 and GIRK channels. A notable difference between the $Kiss1^{ARH}$ neurons and the LS neuronal circuitry is that the GIRK channel activity is predominately at the nerve terminal of $Kiss1^{ARH}$ neurons, and GIRK channels are opened via dynorphin binding to kappa-opioid receptors, which does not translate into membrane hyperpolarization of the soma membrane from which we are recording (Qiu J. et al., 2016). Therefore, although the high frequency firing activity of both LS and $Kiss1^{ARH}$ neurons can be modeled around TRPC and GIRK channels, the generated firing patterns are dramatically different based on the timing (co-incident activation of TRPC4 and GIRK channels in LS) and localization of the GIRK channels in the axon terminal of $Kiss1^{ARH}$ neurons. Moreover, E2-treated, ovariectomized females show a significant down-regulation of both *Trpc5 and Girk2* mRNA expression in $Kiss1^{ARH}$ neurons (**Figure 10**), which is important for the physiological transitioning as described below.

Interestingly, the hypothalamic A12 (ARH) dopamine neurons show a rhythmic “oscillatory” firing behavior that transitions to a tonic firing mode with synaptic input from Thyrotropin-releasing hormone (TRH) neurons (Lyons D.J. et al., 2010) or feedback by circulating prolactin, released by pituitary lactotrophs (Lyons D. J. et al., 2012). A more recent paper has revealed that TRPC5 channels mediate the plateau potential and tonic firing in A12 dopamine neurons in response to prolactin (Blum et al., 2019). Similar to our findings with CRISPR deletion of Trpc5 in $Kiss1^{ARH}$ neurons (**Figures 11 and 12**), conditional knockout of Trpc5 in dopamine neurons abrogated the prolactin-induced plateau potential and tonic firing. Although Blum and colleagues did not model the oscillatory firing or tonic firing of the A12 dopamine neurons, their findings are consistent with our results showing that the activation of TRPC5 channels underlies the slow EPSP (plateau potential) and sustained firing.

## Contribution of endogenous $K^+$ channels to synchronized and burst firing

Beyond the ligand-gated (e.g., baclofen) GIRK channels, there are endogenous $K^+$ channels that help sculpt the firing activity of kisspeptin neurons. We focused on the calcium-activated $K^+$ channel family: the large-conductance, calcium-activated potassium (BK, also called $BK_{Ca}$, $K_{Ca}1.1$, MaxiK, *Slo*), small conductance, calcium-activated $K^+$ (SK1, SK2, SK3) (Bond et al., 2005), and the $K^+$ channels underlying the M-current (KCNQ, Kv7.1-7.5) (Brown and Passmore, 2009), which mediate the fast afterhyperpolarization (AHP), the intermediate AHP/slow AHP, respectively (Andrade et al., 2012)

BK channels are gated by both voltage and cytoplasmic calcium and sculpt action potential firing in CNS neurons (Blatz and Magleby, 1987; Marty, 1989; Sah P., 1996; Storm, 1990). Indeed, BK channels have been shown to mediate rapid spike repolarization—*i.e.*, the fast AHP in hippocampal CA1 pyramidal neurons (Lancaster and Nicoll, 1987; Storm, 1987). Blockade of BK channels in CA1 neurons attenuates the initial discharge frequency in response to current injection, which is attributable to suppression of the BK channel-dependent rapid spike repolarization (Lancaster and Nicoll, 1987; Storm, 1987). Blockade of BK channels is thought to increase inactivation of the spike-generating transient $Na^+$ current and activate more of the slower $K^+$ currents, thereby enhancing refractoriness and reducing excitability during the immediate aftermath of the first action potential (Shao et al., 1999). Thus, BK channels facilitate high-frequency burst firing of CA1 neurons. Furthermore, extracellular field recordings confirmed that BK channels contribute to high-frequency burst firing in response to excitatory synaptic input to distal dendrites in CA1 neurons (Gu et al., 2007). Therefore, BK channels appear to play an

important role for early high-frequency, rapidly adapting firing in hippocampal CA1 pyramidal neurons, thus promoting the type of bursting that is characteristic of these cells *in vivo* during behavior. Based on our *in vitro* electrophysiological recordings and computational modeling we see a similar physiological phenomenon in Kiss1$^{ARH}$ neurons (**Figure 8**). Not only does E2 increase the mRNA expression of *Kcnma1* (**Figure 8G**), but also the maximum BK (IbTx-sensitive) current by 4-fold. In addition, *Kcnb1* mRNA was also up-regulated, and the combination of these two $K^+$ conductances would facilitate rapid repolarization during burst firing and promote glutamate release similar to hippocampal CA1 neurons.

In contrast to BK channel expression, E2 did not affect the mRNA expression of SK3 channel mRNA. SK channels underlie the apamin-sensitive component of the medium duration AHP and are responsible for repolarization following a burst of action potentials (Andrade et al., 2012; Bond et al., 2005). The activation of SK channels is voltage-independent, but SK channels have a higher affinity for $Ca^{2+}$ than BK channels (Andrade et al., 2012). SK channels are tightly coupled (within 100 nm) to L-type $Ca^{2+}$ channels, and BK channels (within 30 nm) are tightly coupled to N-type $Ca^{2+}$ channels in hippocampal CA1 pyramidal neurons (Marrion and Tavalin, 1998). The determination of the proximity of SK and BK channels to HVA calcium channels in kisspeptin neurons will require cell-attached patch recordings. However, in Kiss1$^{ARH}$ neurons the SK channels may come into play during a short burst of action potentials but would become overwhelmed with the higher frequency synchronized, sustained firing as a result of NKB stimulation (Qiu J. et al., 2016). As discussed above what limits the synchronized firing of Kiss1$^{ARH}$ neurons is the activation of GIRK channels.

Finally, the calcium-activated slow AHP probably plays a critical role in the repolarization of Kiss1$^{ARH}$ after burst firing. The molecular identification of the channels mediating the slow AHP has long been an area of intense investigation (Andrade et al., 2012; Vogalis et al., 2003). A critical feature of the slow AHP is that it activates very slowly (hundreds of milliseconds) long after the rise in cytoplasmic $Ca^{2+}$ (Sah P. and Clements, 1999) so an intermediate $Ca^{2+}$ signaling molecule has long been thought to be involved. Indeed, Tzingounis and colleagues (Tzingounis A.V. et al., 2007) have provided compelling evidence that the diffusible calcium sensor hippocalcin is the critical intermediate molecule involved in $Ca^{2+}$ sensing. The slow AHP is abrogated in hippocalcin KO mice, and transfection of hippocalcin into cultured hippocampal neurons generates a pronounced slow AHP in response to a depolarizing stimulus (Tzingounis A.V. et al., 2007). Importantly, the slow AHP is activated by $Ca^{2+}$ with an $EC_{50}$ ≈ 300 nM, which is well within the operational range of hippocalcin but well below that of calmodulin (Andrade et al., 2012). Finally, two seminal papers from Tzingounis and colleagues demonstrate that KCNQ 2, 3 channels are responsible for the slow AHP in hippocampal dentate neurons (Tzingounis A. V. and Nicoll, 2008), and KCNQ 5 channels are responsible for the slow AHP in CA3 neurons (Tzingounis A. V. et al., 2010). Moreover, the KCNQ channel blocker XE991 attenuates the slow AHP in CA3 neurons (Tzingounis A. V. and Nicoll, 2008). Based on these seminal findings we investigated the role of the KCNQ channels, which "classically" underlie the M-current in Kiss1$^{ARH}$. The M-current was first identified in Kiss1$^{ARH}$ neurons by Conde and Roepke (Conde and Roepke, 2019), and presently we found that *Kcnq2* mRNA is expressed in Kiss1$^{ARH}$ neurons and up-regulated by E2, which translated into a greater M-current in Kiss1$^{ARH}$ neurons (**Figure 9**). Incorporating the M-current into our computational model indeed supports our hypothesis that this is a critical $K^+$ conductance, along with SK and BK, for membrane repolarization after burst firing (**Figure 9G**). Importantly the slow AHP, as opposed to the fast AHP (BK) and medium AHP (SK) is highly regulated by multiple neurotransmitters (Andrade et al., 2012), which sets the stage for further modulation of the slow EPSP in Kiss1$^{ARH}$ neurons.

## Importance of E2-driven physiological transitioning

Since the expression of the peptide neurotransmitters in Kiss1$^{ARH}$ neurons are down-regulated by E2, the Kiss1$^{ARH}$ neurons are believed to be under "inhibitory" control by E2 and are important for "negative-feedback" regulation of GnRH release (Lehman et al., 2013; Navarro V. M. et al.,

2009; Smith et al., 2005) (Rance Naomi E. and Young, 1991) (Rance N.E., 2009). However, our past (Gottsch et al., 2011) and current findings document that these Kiss1$^{ARH}$ neurons express HVA and LVA calcium and HCN (pacemaker) channels and are excited by co-released glutamate from neighboring Kiss1$^{ARH}$ neurons, which indicates that these neurons have pacemaker electrophysiological properties similar to other CNS neurons (Bal and McCormick, 1993; Lüthi and McCormick, 1998). Additionally, in contrast to the neuropeptides, E2 increases *Slc17a6* (*Vglut2*) mRNA expression, in addition to mRNA for the voltage-activated calcium and HCN channels, and increases glutamate release onto Kiss1$^{AVPV/PeN}$ neurons (Qiu J. et al., 2018). Interestingly, *Slc17a6* mRNA expression in Kiss1$^{ARH}$ neurons and the probability of glutamate release are decreased along with the neuropeptides in intact versus castrated males (Nestor et al., 2016), which indicates a profound sex difference in the glutamate signaling by Kiss1$^{ARH}$ neurons (Nestor et al., 2016; Qiu J. et al., 2018). Obviously, in the male there is no preovulatory LH surge so there is no need for excitatory glutamatergic input to the few Kiss1$^{AVPV}$ neurons in the male.

In females, conditional knockout of *Slc17a6* in Kiss1 neurons abrogates glutamate release from Kiss1$^{ARH}$ neurons (Qiu J. et al., 2018). Kiss1$^{AVPV/PeN}$ neurons do not express *Slc17a6* and do not release glutamate. Within the Kiss1$^{ARH}$ neurocircuitry the lack of glutamate transmission does not diminish the slow EPSP in ovariectomized females (Qiu J. et al., 2018). Indeed, a recent publication from the Herbison lab demonstrates that glutamate generates small “synchronizing” events that are dependent on the ionotropic receptors (Han et al., 2023), but the fast neurotransmitter is unable to support the sustained firing (*i.e.*, slow EPSP) that is necessary for peptide release and synchronization of the KNDy network. Rather, we believe that glutamate neurotransmission is more important for excitation of Kiss1$^{AVPV/PeN}$ neurons and facilitating the GnRH (LH) surge with high circulating levels of E2, when peptide neurotransmitters are at a nadir, but glutamate levels are high in female Kiss1$^{ARH}$ neurons. Indeed, low frequency (5 Hz) optogenetic stimulation of Kiss1$^{ARH}$ neurons, which only releases glutamate in E2-treated, ovariectomized females (Qiu J. et al., 2016), generates a surge-like increase in LH release during periods of optical stimulation (Lin et al., 2021; Voliotis et al., 2021). Therefore, there appears to be a clear role for glutamatergic transmission from the Kiss1$^{ARH}$ to Kiss1$^{AVPV/PeN}$ neurons in amplifying the LH surge in the female mouse. Finally it is important to keep in mind that even in the presence of high physiological levels of E2, the mRNA expression of *Tac2* is many-fold higher than *Kiss1* (**Figure 10**), which is essential for NKB maintaining synchronous firing of Kiss1$^{ARH}$ neurons, albeit at a lower frequency, across all physiological states (Qiu J. et al., 2016). Indeed, there is a progressive change from a strictly pulsatile pattern of GnRH in the hypophyseal portal circulation to one containing both pulsatile and non-pulsatile components during the development of the GnRH surge in the ewe (Evans, Dahl, Mauger, & Karsch, 1995; Evans, Dahl, Mauger, Padmanabhan, et al., 1995), and a pulsatile mode of LH secretion during the preovulatory LH surge is also evident in other species including humans (Rossmanith et al., 1990). Therefore, we believe that our cellular molecular and electrophysiological findings in combination with our computational modelling provide a foundation for understanding the complex role of Kiss1$^{ARH}$ neurons in controlling fertility in the mammal. Finally, our model provides the first comprehensive biophysical description of the conductances underlying the neuronal activity of Kiss$^{ARH}$ neurons, which can serve as a basis for future computational modelling of the Kiss$^{ARH}$ neuronal network and its interactions with other brain regions involved in the complex regulation of mammalian female reproduction.

# Methods and Materials

## Animals

All the animal procedures described in this study were performed in accordance with institutional guidelines based on National Institutes of Health standards and approved by the Institutional Animal Care and Use Committee at Oregon Health and Science University (OHSU) or in accordance with the United Kingdom Animals (Scientific Procedures) Act 1986 and were approved by King's College London (KCL) Ethical Review Committee.

## Mice

*Kiss1*$^{Cre}$ transgenic female mice version 2 (Padilla et al., 2018) were selectively bred at OHSU and KCL. They also were crossed with heterozygous Ai32 mice (RRID:IMSR_JAX:024109, C57BL/6 background) which carry ChR2 (H134R)–EYFP gene in their Gt(ROSA)26Sor locus (Madisen et al., 2012). All animals were maintained under controlled temperature and photoperiod (lights on at 0600h and off at 1800h at OHSU or 0700h and off at 1900h at KCL) and given free access to food (Lab Diets 5L0D) and water. Where specified, Kiss1$^{Cre}$ mice received viral injections to express channelrhodopsin 2 (ChR2) in Kiss1$^{ARH}$ neurons, fourteen to twenty-one days prior to each experiment as described (Qiu J. et al., 2016). Some of the females were ovariectomized seven days prior to an experiment. Each animal was injected on day 5 following OVX with 0.25 µg E2 or vehicle, followed on day 6 with 1.50 µg E2 or vehicle and used for experiments on day 7 (Bosch et al., 2013).

## AAV delivery to Kiss1$^{Cre}$ mice

Fourteen to twenty-one days prior to each experiment, the *Kiss1*$^{Cre}$ mice (>60 d old) received bilateral ARH injections of a Cre-dependent adeno-associated viral (AAV; serotype 1) vector encoding mCherry (AAV1-Ef1α-DIO-mCherry) or AAV1 vectors designed to encode SaCas9 and single-guide RNAs (sgRNAs) (See the SaCas9 section for specifics on the sgRNA design). Using aseptic techniques, anesthetized female mice (1.5% isoflurane/$O_2$) received a medial skin incision to expose the surface of the skull. The glass pipette with a beveled tip (diameter = 45 µm) was filled with mineral oil, loaded with an aliquot of AAV using a Nanoject II (Drummond Scientific). ARH injection coordinates were anteroposterior (AP): −1.20 mm, mediolateral (ML): ± 0.30 mm, dorsoventral (DV): −5.80 mm (surface of brain z = 0.0 mm); 500 nl of the AAV ($2.0\times10^{12}$ particles/ml) was injected (100 nl/min) into each position, and the pipette left in place for 10 min post-injection, then slowly retracted from the brain. The skin incision was closed using Vetbond (3M) and each mouse received analgesia (Rimadyl, 4-5 mg/kg, *s.c.*).

## Generation of AAV1-FLEX-SaCas9-U6-sgTrpc5

The generation of AAV1-FLEX-SaCas9-U6-sg*Trpc5* viruses were done at the University of Washington using published methods (Gore et al., 2013; Hunker et al., 2020). The constructs of sgRNAs for *Trpc5* (AAV1-FLEX-SaCas9-U6sg*Trpc5*) were designed to target exon2 and exon7, respectively (**Figure 11A and B**). To achieve *Trpc5* mutagenesis in Kiss1$^{ARH}$ neurons, Kiss1$^{Cre}$ mice were co-injected with AAV1-DIO-mCherry, AAV1-FLEX-SaCas9-U6-sg*Trpc5*-exon2, and AAV1-FLEX-SaCas9-U6-sg*Trpc5*-exon7 at a ratio of 10%, 45%, and 45%, respectively. Control animals were co-injected with AAV1-FLEX-SaCas9-U6-sg*Rosa26* and AAV1-DIO-mCherry at a ratio of 90% and 10%, respectively. AAV1-DIO-mCherry was co-injected with Cas9 vectors to confirm the targeting of injections and visualize the infected Kiss1$^{ARH}$ neurons.

## Visualized whole-cell patch recording

Electrophysiological and optogenetic studies were made in coronal brain slices (250 μm) containing the ARH from AAV1-EF1α-DIO-mCherry injected Kiss1Cre:GFP or Kiss1-Cre:EYFP::AI32 mice, which were vehicle-treated OVX, and E2-treated OVX females 10 weeks and older as previously described (Qiu J. et al., 2016; Qiu J. et al., 2018). Whole-cell patch recordings were performed in voltage-clamp and current-clamp as previously described (Qiu J. et al., 2018) using an Olympus BX51 W1 fixed stage scope out-fitted with epifluorescence and IR-DIC video microscopy. Patch pipettes (A-M Systems; 1.5 μm outer diameter borosilicate glass) were pulled on a Brown/Flaming puller (Sutter Instrument, model P-97) and filled with the following solution: 128 mM potassium gluconate, 10 mM NaCl, 1 mM $MgCl_2$, 11 mM EGTA, 10 mM HEPES, 2 mM ATP, and 0.25 mM GTP adjusted to pH 7.3 with KOH; 295 mOsm. Pipette resistances ranged from 3.5–4 MΩ. In whole-cell configuration, access resistance was less than 30 MΩ; the access resistance was 80% compensated. The input resistance was calculated by measuring the slope of the I-V relationship curve between −70 and −50 mV. Standard whole-cell patch recording procedures and pharmacological testing were performed as previously described (Qiu J. et al., 2003; Qiu J. et al., 2014). Electrophysiological signals were digitized with a Digidata 1322A (Axon Instruments) and the data were analyzed using p-Clamp software (Molecular Devices, Foster City, CA). The liquid junction potential was corrected for all data analysis.

For optogenetic stimulation, a light-induced response was evoked using a light-emitting diode (LED) 470 nm blue light source controlled by a variable 2A driver (ThorLabs, Newton, NJ) with the light path directly delivered through an Olympus 40x water-immersion lens. For high-frequency (20 Hz) stimulation the length of stimulation was 10 seconds (Qiu J. et al., 2016).

For studying the activation/inactivation characteristics of the $Ca^{2+}$ current, the electrodes were filled with an internal solution as described (Qiu J. et al., 2003) consisting of the following (in mM): 100 $Cs^+$ gluconate, 20 TEA-Cl, 10 NaCl, 1 $MgCl_2$, 10 HEPES, 11 EGTA, 1 ATP, 0.25 GTP, the pH was adjusted to 7.3 with CsOH at 300 mOsm. The bath solution as described (Zhang X. B. and Spergel, 2012) consisted of (in mM) 117.5 NaCl, 25 $NaHCO_3$, 1.25 $NaH_2PO_4$, 10 TEA-Cl, 2 $CaCl_2$, 1 $MgCl_2$, 20 sucrose and 5 glucose, gassed with 95% $O_2$ /5% $CO_2$ (pH 7.4, 309 mOsm) and supplemented with 1 μM TTX, 10 μM CNQX, 50 μM AP5 and 100 μM picrotoxin. The effects of estrogen treatment on the peak current, peak current density, and activation/inactivation characteristics of calcium current were measured. Activation curves were fitted by the Boltzmann equation: $I/I_{max}=1/\{1+\exp[V_{1/2}-Vs)/k]\}$, where I is the peak current at the step potential Vs, Imax is the peak current amplitude, $V_{1/2}$ is the step potential yielding half-maximum current, and k is the slope factor. Inactivation curves were fit with the Boltzmann equation: $I/I_{max} = 1 - 1/\{1 + \exp[(V_H - V_{1/2})/k]\}$, where I is the peak current at the step potential $V_H$, $I_{max}$ is the peak current amplitude, $V_{1/2}$ is the step potential at which half the current is inactivated, and k is the slope factor.

To record M-currents, pipettes were filled with an internal solution consisting of 10 mM NaCl, 128 mM K-gluconate, 1 mM MgCl, 10 mM HEPES, 1 mM ATP, 1.1 mM EGTA, and 0.25 mM GTP (pH 7.3; 290 mOsm). During voltage-clamp, we employed a standard deactivation protocol (Conde and Roepke, 2019; Roepke et al., 2011) to measure potassium currents. This involved 500-ms voltage steps ranging from –30 to –75 mV in 5-mV increments, following a 300-millisecond prepulse to –20 mV. The amplitude of the M-current relaxation or deactivation was quantified as the difference between the initial (<10 ms) and sustained current (>475 ms) of the current trace.

The bath solution for whole-cell recording of BK, SK and M currents was aCSF supplemented with 1 μM TTX, 10 μM CNQX, 50 μM AP5 and 100 μM picrotoxin.

## Electrophysiological solutions/drugs

A standard artificial cerebrospinal fluid (aCSF) was used (Qiu J. et al., 2003; Qiu J. et al., 2010). All drugs were purchased from Tocris Bioscience unless otherwise specified. 1 mM TTX (Alomone Labs), 50 mM DL-2-Amino-5-phosphonopentanoic acid sodium salt (AP5), 10 mM 6-Cyano-7-nitroquinoxaline-2,3-dione disodium (CNQX), 100 mM picrotoxin, 10 mM Nifedipine (Sigma), 2 mM ω-conotoxin GVIA (ConoGVIA; Alomone Labs), 0.5 mM ω-conotoxin MVIIC (ConoMVIIC; Alomone Labs, 50 µM ω-agatoxin IVA (AgaIVA; Alomone Labs), 50 µM SNX-482 (Alomone Labs), 10 mM TTA-P2 (TTAP2; Alomone Labs), 200 mM $CdCl_2$ ($Cd^{2+}$; Sigma), 40 mM XE991 (Alomone Labs), 100 µM Iberiotoxin (Alomone Labs), 500 µM Apamin (Alomone Labs) and 100 mM $NiCl_2$ ($Ni^{2+}$; Sigma). Stocks (1000×) were prepared in dimethylsulfoxide DMSO (picrotoxin, TTAP2) or water (TTX, AP5, CNQX, ConoGVIA, ConoMVIIC, AgaIVA, SNX-482, $Cd^{2+}$, $Ni^{2+}$) and stored at −20°C. Aliquots of the stock solutions were stored as appropriate until needed.

## Cell harvesting of dispersed Kiss1$^{Cre}$ neurons and real-time quantitative PCR (qPCR)

Cell harvesting and qPCR was conducted as previously described (Bosch et al., 2013). The ARH was microdissected from basal hypothalamic coronal slices obtained from female Kiss1$^{Cre}$ version 2 mice (Padilla et al., 2018) (n = 5-7 animals/group). The dispersed cells were visualized, patched, and then harvested (5 or 10 cells/tube) as described previously (Bosch et al., 2013). Briefly, ARH tissue was incubated in papain (7mg/ml in oxygenated aCSF) for 50 min at 37° C then washed 4 times in low $Ca^{2+}$ aCSF and two times in aCSF. For cell dispersion, Pasteur pipettes were flame polished to decreasing tip sizes and gentle trituration used to disperse the neurons onto a glass bottom dish. The plated cells were bathed in oxygenated aCSF using a peristaltic pump to keep the cells viable and clear of debris. Healthy cells with processes and a smooth cell membrane were harvested. Pipettes (World Precision Instruments; 1.5 µm outer diameter borosilicate glass) were pulled on a Brown/Flaming puller (Sutter Instrument, model P-87) to a 10 µm diameter tip. The cells were harvested using the XenoWorks Microinjector System (Sutter Instruments, Navato, CA) which provides negative pressure in the pipette and fine control to draw the cell up into the pipette. Cell pools were harvested and stored at -80°C. All cell pools were DNAse-treated using DNase1. cDNA synthesis was performed as previously described (Bosch et al., 2013).

Primers for the genes that encode for low and high voltage-gated calcium channels, TRPC5, Vglut2, large conductance calcium-activated $K^+$ (BKα) channels, small conductance calcium-activated $K^+$ (SK3) channels and GAPDH were designed using Clone Manager software (Sci Ed Software) to cross at least one intron-exon boundary and optimized as previously described using Power Sybr Green method (Bosch et al., 2013). We have already published primer sequences for the low voltage-activated calcium channels, Vglut2 and GAPDH (see **Table 1**) (Qiu J. et al., 2018). Real-time qPCR controls included neuronal pools without reverse transcriptase (-RT), hypothalamic RNA with RT (+) and without RT (-), as well as water blanks. Standard curves using ARH cDNA were utilized to determine the real-time PCR efficiency ($E = 10^{(-1/m)} - 1$) (Biosystems, 2006; Pfaffl, 2001). Only primers resulting in efficiencies of 90-100% were used for analysis. Primer sequences, qPCR parameters and efficiency calculations are provided in **Table 1**.

## mRNA expression analysis

qPCR was performed on a Quantstudio 7 Flex Real-Time PCR System (Applied Biosystems) using Power SYBR Green PCR Master Mix (Applied Biosystems) according to established protocols (Bosch et al., 2013). The comparative $\Delta\Delta C_T$ method (Livak and Schmittgen, 2001; Pfaffl, 2001; Schmittgen and Livak, 2008) was used to determine values from duplicate samples of 4 µl for the target genes and 2 µl for the reference gene *GAPDH* in a 20 µl reaction volume containing 1x Power SYBR Green PCR Master Mix and 0.5 µM forward and reverse primers. Three to four 5-cell or 10-cell pools per animal were analyzed from 5-7 animals per group. The relative linear quantity

was determined using the $2^{-\Delta\Delta CT}$ equation (Livak and Schmittgen, 2001; Pfaffl, 2001; Schmittgen and Livak, 2008). Relative mRNA expression level of target genes in Kiss1$^{Cre}$ neurons was obtained by comparing OVX Oil-treated controls to OVX E2-treated animals. The mean Δ CT for the target genes from the OVX Oil-treated control samples was used as the calibrator. The data were expressed as *n*-fold change in gene expression normalized to the reference gene *GAPDH* and relative to the calibrator.

## Experimental design and Statistical analysis

For the visualized, whole-cell patch recording experiments, only one cell was recorded per slice. Two to three slices were analyzed from each Kiss1$^{Cre}$ mouse, with at least 3-5 mice contributing to each group. For cell harvesting of dispersed Kiss1$^{Cre}$-YFP neurons and qPCR measurements, 10 cells per pool and 3-6 pools from each animal were used, unless otherwise specified. Statistical comparisons between two groups were performed using an unpaired two-tailed Student's t-test. Comparisons between more than two groups were performed using the repeated measures, multifactorial ANOVA. If a significant interaction was encountered, we then moved to the one-way ANOVA, followed by the multiple range tests as specified in the appropriate figure legends. All data were analyzed using GraphPad Prism version 6. All data are presented as mean ± standard error of the mean (SEM). Differences were considered statistically significant if the probability of error was less than 5%.

## Mathematical model and simulation of neuronal behavior

A mathematical model of the Kiss1$^{ARH}$ neuron was developed and calibrated based on our physiological findings. Here, we employed the Hodgkin-Huxley modelling approach (Hodgkin and Huxley, 1952). Accordingly, the equation describing the membrane potential $V_m$ of the Kiss1$^{ARH}$ neuron is given by

$$C_m \frac{dV_m}{dt} = -I,$$

where $C_m$ is the membrane capacitance and $I$ is the sum of 12 ionic currents:

$$I = I_{NaT} + I_{NaP} + I_A + I_{BK} + I_h + I_{SK} + I_M + I_T + I_{Ca} + I_{TRPC5} + I_{GRIK} + I_{leak}$$

$I_{NaT}$ and $I_{NaP}$ are the transient and persistent sodium currents, respectively; $I_A$ represents the A current; $I_M$ represents the M current; $I_{SK}$ and $I_{BK}$ are the potassium currents through the SK and BK channels respectively; $I_h$ the HCN current; $I_T$ the T-type calcium current; $I_{Ca}$ represents other calcium currents (L-, N-, P/Q-, and R-type); $I_{TRPC5}$ represents Calcium current throught the TRPC5 channel; $I_{GIRK}$ potassium current through the GIRK channels. Finally, $I_{leak}$ represents the contribution of leak currents. We use the Hodgkin-Huxley formalism to model current dynamics and their dependence on the membrane potential. A complete specification of all currents along with the complete table of model parameters can be found in the supplementary material. Model simulations were conducted in Matlab using the built-in numerical solver (ode45; based on an explicit Runge-Kutta (4, 5) formula). The Matlab code is available at *https://git.exeter.ac.uk/mv286/kiss1-arcuate-neuron-model*.

# Acknowledgements

# Funding

All electrophysiology and molecular biological studies were funded by the National Institutes of Health Grant R01-DK698098 (OKR and MJK, multi-PI). The generation of the *sgRNA's* was funded by National Institutes of Health Grants P30-MH048736 and R01104450 (LSZ). The computational modeling was funded by the BBSRC via grant BB/W0058831/1 (KTA and MV) and the EPSRC via grant EP/T017856/1 (KTA). The *in vivo* hormone measurements were funded by the BBSRC via grant BB/W005913/1 (KOB and XFLi). The BBSRC also provided an International Partnership Award, BB/3019978/1, to facilitate collaboration between the UK partners (KOB, XFLi, KTA and MV) and the USA partners (MJK, OKR, JQ and MAB).


# Author contributions

JQ designed, performed and analyzed the electrophysiological experiments and did the viral injections; MV performed the computational modeling and wrote the code; MAB designed, performed and analyzed the single cell harvesting and qPCR experiments; XFLi designed and performed the *in vivo* hormone measurements; LSZ designed the *sgRNAs* against *TRPC5;* KTA provided resources for modeling; KOB provided laboratory space and resources to conduct the *in vivo* experiments; MJK and OKR conceived and designed the study, provided laboratory space and resources to conduct the experiments and wrote the manuscript with input from all the contributing authors.

# Supplementary Information

## A mathematical model of the arcuate nucleus kisspeptin neuron

A schematic diagram of the Arcutate nucleus Kiss1 (Kiss1$^{ARH}$) neuron model is presented in **Fig. S1** and parameter values used in the simulations are given in Table S1.

The equation describing the membrane potential, $V_m$, of Kiss1$^{ARH}$ is given by

$$C_m \frac{dV_m}{dt} = -I,$$

where $C_m$ is the membrane capacitance and $I$ is the sum of 12 ionic currents:

$$I = I_{NaT} + I_{NaP} + I_A + I_{BK} + I_h + I_{SK} + I_M + I_T + I_{Ca} + I_{TRPC5} + I_{GIRK} + I_{leak}$$

$I_{NaT}$ and $I_{NaP}$ are the transient and persistent sodium currents, respectively; $I_A$ represents the A current; $I_M$ represents the M current; $I_{SK}$ and $I_{BK}$ are the potassium currents through the SK and BK channels respectively; $I_T$ the T-type calcium current; $I_{Ca}$ represents other calcium currents (L-, N-, P/Q-, and R-type); $I_{TRPC5}$ represents Calcium current throught the TRPC5 channel; $I_{GIRK}$ potassium current through the GIRK channels. Finally, $I_{leak}$ represents the contribution of leak currents.

We use the Hodgkin-Huxley formalism to model current dynamics and their dependence on the membrane potential. Below we detail are the equations governing the currents.

## Transient sodium current

$$I_{NaT} = g_{NaT} \cdot m_{NaT,\infty}(V_m) \cdot h_{NaT} \cdot (V_m - E_{Na}),$$

where $g_{NaT}$ is the maximum conductance; $E_{Na}$ is the sodium reversal potential; $h_{NaT}$ is the inactivation gating variable that obeys the following equation:

$$\frac{dh_{NaT}}{dt} = \frac{h_{NaT,\infty}(V_m) - h_{NaT}}{\tau_{h,NaT}}.$$

Parameter $\tau_{h,NaT}$ dictates the timescale of inactivation and $h_{NaT,\infty}(V_m)$ is the steady-state inactivation function:

$$h_{NaT,\infty}(V_m) = \frac{1}{1+e^{-(V_m - V_{h,NaT})/k_{h,NaT}}}.$$

Parameter $V_{h,NaT}$ describes the voltage achieving half-maximal inactivation and parameter $k_{h,NaT}$ is the associated scaling function.

Finally, in the current formulation $m_{NaT,\infty}(V_m)$ is the steady-state activation function given by:

$$m_{NaT,\infty}(V_m) = \frac{1}{1+e^{-(V_m - V_{m,NaT})/k_{m,NaT}}}.$$

The transient sodium channel is modelled using parameter values from the Purkinje neuron [**1**]. This neuron was chosen as a baseline as it contains the same subunits, i.e., NaV1.1-α, NaV1.2-α, and NaV1.6-α [**1**], as the transient sodium channel in arcuate Kiss1 neuron [**2**].

## Persistent sodium current

$$I_{NaP} = g_{NaP} \cdot m_{NaP,\infty}(V_m) \cdot h_{NaP} \cdot (V_m - E_{Na}),$$

$g_{NaP}$ is the maximum conductance; $h_{NaP}$ is the corresponding inactivation gating variable that obeys the following equation:

$$\frac{dh_{NaP}}{dt} = \frac{h_{NaP,\infty}(V_m) - h_{NaP}}{\tau_{h,NaP}};$$

and the steady-state activation and inactivation functions are given by:

$$m_{NaP,\infty}(V_m) = \frac{1}{1 + e^{-(V_m - V_{m,NaP})/k_{m,NaP}}},$$
$$h_{NaT,\infty}(V_m) = \frac{1}{1 + e^{-(V_m - V_{h,NaP})/k_{h,NaP}}}.$$

The above description of the persistent sodium current was taken from a model of the GnRH neuron [**3**].

## A current

$$I_A = g_A \cdot m_A \cdot h_A \cdot (V_m - E_K)$$

$g_{NaP}$ denotes the maximum conductance; $E_K$ is the potassium reversal potential; and $m_A$ and $h_A$ are the corresponding activation and inactivation gating variables, which are described by the following equations:

$$\frac{dm_A}{dt} = \frac{m_{A,\infty}(V_m) - m_A}{\tau_{m,A}};$$
$$\frac{dh_A}{dt} = \frac{h_{A,\infty}(V_m) - h_A}{\tau_{h,A}}.$$

The steady-state activation and inactivation functions are given by:

$$m_{A,\infty}(V_m) = \frac{1}{1 + e^{-(V_m - V_{m,A})/k_{m,A}}},$$
$$h_{A,\infty}(V_m) = \frac{1}{1 + e^{-(V_m - V_{h,A})/k_{h,A}}}.$$

The model of the A-current was based on Mendonca's model of Kv4 channels [**4**], as these channels are also found in arcuate Kiss1 neurons [**5**].

## BK current

$$I_{BK} = g_{BK} \cdot b_{BK,\infty}(V_m, c) \cdot (V_m - E_K),$$

Here, $g_{BK}$ is the maximum conductance; and $b_{BK,\infty}(V_m, c)$ is the steady-state activation function that depends on the membrane potential, $V_m$, as well as on the cytosolic calcium concertation, $c$:

$$b_{BK,\infty}(V_m, c) = \frac{1}{1 + e^{-(V_m - V_{BK}(c))/k_{BK}}},$$
$$V_{BK}(c) = V_{BK,0} - k_{shift} \log \frac{c}{k_{c,BK}}.$$

The model of the BK-current was based on the model presented in [**6**], with the conductance parameter fitted to the current-voltage relationships recorded from arcuate Kiss1 neurons in the absence and presence of the specific BK blocker, iberiotoxin.

## SK current

$$I_{SK} = g_{SK} \cdot b_{SK,\infty}(c) \cdot (V_m - E_K)$$

$g_{SK}$ denotes the maximum conductance; and $b_{SK,\infty}(c)$ is the steady-state activation function, which depends on the cytosolic calcium concertation, $c$:

$$b_{SK,\infty}(c) = \frac{c^n}{c^n + K_{SK}^n}.$$

The model of the BK-current was based on the model presented in [**7**], with the conductance fitted to the current-voltage relationships recorded from arcuate Kiss1 neurons in the absence and presence of the specific SK blocker, apamin.

## M current

$$I_M = g_M \cdot m_M \cdot (V_m - E_K)$$

$g_M$ denotes the maximum conductance, and $m_M$ is the corresponding activation gating variable:

$$\frac{dm_M}{dt} = \frac{m_{M,\infty}(V_m) - m_M}{\tau_{m,M}}$$

with the steady-state activation function, $m_{M,\infty}(V_m)$, taking the form:

$$m_{A,\infty}(V_m) = \frac{1}{1 + e^{-(V_m - V_{m,A})/k_{m,A}}}.$$

The model of the M-current was parameterised using the steady-state voltage-clamp measurements from actuate Kiss1 neurons [**8**], while for the activation timescale we used the timescale used in a model of the CA1/3 pyramidal cells [**9**].

## h currents

$$I_h = g_h \cdot \left[p_h \cdot m_{h,1} + (1 - p_h) \cdot m_{h,2}\right] \cdot (V_m - E_h),$$

$g_h$ denotes the maximum conductance; and $m_{h,1}$ and $m_{h,2}$ are separate activation gating variables operating on different timescales ($\tau_{m,h,1}$ and $\tau_{m,h,2}$ respectively):

$$\frac{dm_{h,1}}{dt} = \frac{m_{h,1,\infty}(V_m) - m_{h,1}}{\tau_{m,h,1}}$$
$$\frac{dm_{h,2}}{dt} = \frac{m_{h,2,\infty}(V_m) - m_{h,2}}{\tau_{m,h,2}}$$

The corresponding steady-state activation functions are:

$$m_{h,1,\infty}(V_m) = \frac{1}{1 + e^{-(V_m - V_{m,h,1})/k_{m,h,1}}},$$
$$m_{h,2,\infty}(V_m) = \frac{1}{1 + e^{-(V_m - V_{m,h,2})/k_{m,h,2}}}.$$

Finally, parameter $p_h$ dictates the relative contribution of and $m_{h,1}$ and $m_{h,2}$ to the total current.

This model of the h-current is based on the hippocampal CA1 pyramidal neuron [**7**].

## T-type calcium current

$$I_T = g_T \cdot m_{T,\infty} \cdot \left[p_T \cdot h_{T,1} + (1 - p_T) \cdot h_{T,2}\right] \cdot (V_m - E_{Ca}),$$

$g_T$ is the maximum conductance; and $h_{T,1}$ and $h_{T,2}$ are separate inactivation gating variables operating on different timescales ($\tau_{h,T,1}$ and $\tau_{h,T,2}$ respectively):

$$\frac{dh_{h,1}}{dt} = \frac{h_{T,1,\infty}(V_m) - h_{T,1}}{\tau_{h,T,1}}$$
$$\frac{dh_{h,2}}{dt} = \frac{h_{T,2,\infty}(V_m) - h_{T,2}}{\tau_{h,T,2}}$$

The corresponding steady-state inactivation functions are:

$$h_{T,1,\infty}(V_m) = \frac{1}{1 + e^{-(V_m - V_{h,T,1})/k_{h,T,1}}},$$
$$h_{T,2,\infty}(V_m) = \frac{1}{1 + e^{-(V_m - V_{h,T,2})/k_{h,T,2}}}.$$

The steady-state activation function is given by:

$$m_{T,\infty} = \frac{1}{1 + e^{-(V_m - V_{m,T})/k_{m,T}}}.$$

Finally, parameter $p_T$ dictates the relative contribution of and $h_{T,1}$ and $h_{T,2}$ to the total current.

To model of the T-current was based on AVPV kisspeptin neurons data presented in [**2**, 10].

## L-, N-, P/Q-, R-type calcium currents

$$I_{Ca} = g_h \cdot m_{Ca} \cdot h_{Ca} \cdot (V_m - E_{Ca})$$

$g_{Ca}$ denotes the maximum conductance; and $m_{Ca}$ and $h_{Ca}$ are the corresponding activation and inactivation gating variables, which are described by the following equations:

$$\frac{dm_{Ca}}{dt} = \frac{m_{Ca,\infty}(V_m) - m_{Ca}}{\tau_{m,Ca}};$$
$$\frac{dh_{Ca}}{dt} = \frac{h_{Ca,\infty}(V_m) - h_{Ca}}{\tau_{h,Ca}}.$$

The steady-state activation and inactivation functions are given by:

$$m_{Ca,\infty}(V_m) = \frac{1}{1 + e^{-(V_m - V_{m,Ca})/k_{m,Ca}}},$$
$$h_{Ca,\infty}(V_m) = \frac{1}{1 + e^{-(V_m - V_{h,Ca})/k_{h,Ca}}}.$$

Parameters of the model for the high voltage activated calcium channels were fitted to the current-voltage relationships obtained from arcuate Kiss1 neuron (see **Figure 7** main text).

## TRPC5 current

$$I_{TRPC5} = g_{TRPC5} \cdot b_{TRPC5}(c, R_{TRPC5,act}) \cdot (V_m - E_{TRPC5})$$

$g_{TRPC5}$ denotes the maximum conductance; and $b_{TRPC5}(c, R_{TRPC5,act})$ the activating gating variable that depends both on cytosolic calcium concertation ($c$) and on NKB-mediated activation of an intermediary effector, $R_{TRPC5,act}$ [**11**]:

$$b_{TRPC5}(c, R) = \frac{R_{TRPC5,act}}{1 + e^{-(c - c_{TRPC5})/k_{TRPC5}}}$$

The dynamics of $R_{TRPC5,act}$ (activated form of $R_{TRPC5}$) are described by:

$$\frac{dR_{TRPC5,act}}{dt} = \left(k_{R_{TRPC5},0} + k_{R_{TRPC5}} \frac{NKB^{n2}}{NKB^{n2} + K_{NKB}^{n2}}\right) \cdot (R_{TRPC5,T} - R_{TRPC5,act}) - k_{-R_{TRPC5}} \cdot R_{TRPC5,act};$$

where NKB is the extracellular NKB concertation; $k_{R,0}$ is the basal rate of $R_{TRPC5}$ activation; $k_R$ is the maximal rate of $R_{TRPC5}$ activation in the presence of NKB; $k_{-R}$ is the rate of $R_{TRPC5}$ inactivation; and $R_{TRPC5,T}$ is the total concentration of the effector.

## GIRK current

$$I_{GIRK} = g_{GIRK} \cdot b_{GIRK}(V_m, R_{GIRK,act}) \cdot (V_m - E_K)$$

$g_{GIRK}$ denotes the maximum conductance; and $b_{GIRK}(V_m, R_{GIRK,act}B)$ the activating gating variable that depends on membrane potential, $V_m$, and on external activation of an intermediary effector, $R_{GIRK,act}$:

$$b_{GIRK}(V_m, R_{GIRK,act}) = m_{GIRK}(V_m)\, R_{GIRK,act}(s)$$

The dynamics of $m_{GIRK}$ are described by:

$$\frac{dm_{GIRK}}{dt} = \frac{m_{GIRK,\infty}(V_m) - m_{GIRK}}{\tau_{GIRK}(V_m)}$$

where the steady state activation function and timescale function are given by:

$$m_{GIRK,\infty}(V_m) = \frac{1}{1 + e^{-\frac{V_m - V_{GIRK}}{k_{GIRK,1}}}} + \frac{\alpha}{1 + e^{-\frac{V_m - V_{GIRK}}{k_{GIRK,2}}}}$$

$$\tau_{GIRK}(V_m) = \frac{1}{\alpha_\tau e^{-(V_m/V_{GIRK})} + \beta_\tau e^{-(V_m/V_{GIRK})}}$$

The dynamics of $R_{GIRK,act}$ are described by:

$$\frac{dR_{GIRK,act}}{dt} = \left(k_{R_{GIRK},0} + k_{R_{GIRK}} \frac{s^{n3}}{s^{n3} + K_s^{n3}}\right) \cdot (R_{GIRK,T} - R_{GIRK,act}) - k_{-R_{GIRK}} \cdot R_{GIRK,act} ;$$

where s is the extracellular concertation of the activation signal. The model and parameters of the GIRK current is taken from [**12**].

## leak currents

$$I_{leak} = I_{leak,0} + I_{leak,Ca} = g_{leak,1} \cdot (V_m - E_K) + g_{leak,2} \cdot (V_m - E_{Ca})$$

## Intracellular calcium dynamics

Finally, the intracellular calcium dynamics are described via the following equation:

$$\frac{dc}{dt} = -\left(I_{Ca} + I_T + I_{TRPC5} + I_{leak,Ca}\right) \cdot \gamma - d_{ca} \cdot c$$

where parameter $\gamma$ converts the currents to molecule fluxes and parameter $d_{ca}$ dictates the linear rate at which calcium is depleted or pumped out of the cell.

### Model Simulation

Integration of the differential equations describing the model was carried out in MATLAB R2023b using a standard 4th order Runge-Kutta method. Parameter fitting was also conducted in MATLAB R2023b using the least squares curve fitting method.

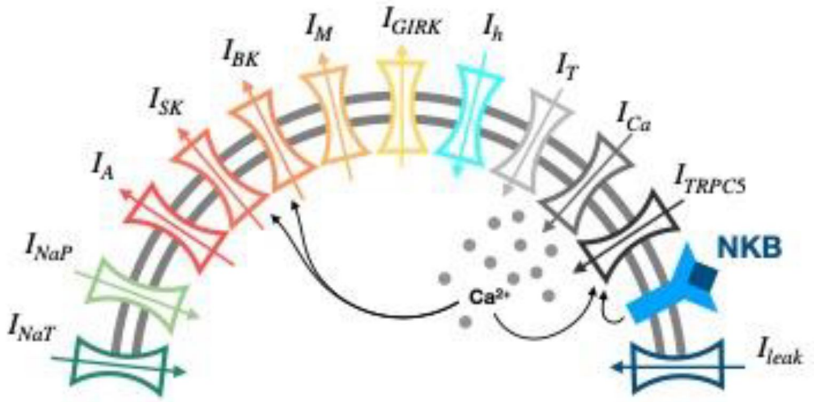


**Figure S1.**

Schematic diagram of the conductance based mathematical model of Arcuate nucleus Kiss1 neurons.

| Model parameters | | | | | |
|---|---|---|---|---|---|
| $C_m$ | 23.13 nF (19.5 in OVX+E2) | | | | |
| Current parameters [1] | | | | | References |
| $I_{NaT}$ | $\tau_{h,NaT}$ | 4.5 ms | $V_{h,NaT}$ | -43.2 mV | [1, 2] |
| | $V_{m,NaT}$ | -25 mV | $k_{m,NaT}$ | 3 mV | |
| | $k_{h,NaT}$ | -8.2 mV | $g_{NaT}$ | 90 nS | |
| | $E_{Na}$ | 66.1 mV | | | |
| $I_{NaP}$ | $\tau_{h,NaP}$ | 250 ms | $V_{h,NaP}$ | -47.4 mV | [3] |
| | $V_{m,NaP}$ | -41.5 mV | $k_{m,NaP}$ | 3 mV | |
| | $k_{h,NaP}$ | -8.5 mV | $g_{NaP}$ | 3.37 nS | |
| | $E_{Na}$ | 66.1 mV | | | |
| $I_A$ | $\tau_{h,A}$ | 10 ms | $V_{h,A}$ | -55.1 mV | [4, 5] |
| | $\tau_{m,A}$ | 20 ms | $V_{m,A}$ | -30 mV | |
| | $k_{h,A}$ | -11.4 mV | $k_{m,A}$ | 10 mV | |
| | $g_A$ | 60 nS in OVX<br>35 in OVX+E2 | $E_K$ | -81 mV | |

**Table S1.**

Table of model parameters.

| | | | | | |
|---|---|---|---|---|---|
| $I_{BK}$ | $k_{BK}$ | 10 mV | $k_{shift}$ | 18 mV | [6] |
| | $V_{BK,0}$ | -22.52 mV | $k_{c,BK}$ | 1.5 μM | |
| | $g_{BK}$ | 13.50 nS in OVX; 20 nS in OVX+E2 | $E_K$ | -81 mV | |
| $I_{SK}$ | $K_{SK}$ | 0.45 μM | $n$ | 4 | [13] |
| | $g_{SK}$ | 28.13 nS in OVX; 26.05 nS in OVX+E2 | $E_K$ | -81 mV | |
| $I_M$ | $\tau_{m,M}$ | 10 ms | $V_{m,M}$ | -50 mV | [8, 9] |
| | $k_{m,M}$ | 20 mV | $g_M$ | 0.23 nS in OVX 1.23 ns in OVX+E2 | |
| | $E_K$ | -81 mV | | | |
| $I_h$ | $\tau_{m,h,1}$ | 80 ms | $V_{m,h,1}$ | -102 mV | [7, 14, 15] |
| | $\tau_{m,h,1}$ | 310 ms | $V_{m,h,2}$ | -102 mV | |
| | $p_h$ | 0.85 | $k_{m,h,1}$ | -10 mV | |
| | $k_{m,h,2}$ | -10 mV | $g_h$ | 0.56 nS (11.23 nS in OVX+E2) | |
| | $E_h$ | -27.8 mV | | | |
| $I_T$ | $\tau_{h,T,1}$ | 1.94 ms | $V_{h,T,1}$ | -69.1 mV | [2, 10] |
| | $\tau_{h,T,2}$ | 86.3 ms | $V_{h,T,2}$ | -69.1 mV | |
| | $p_h$ | 0.5 | $V_{m,T}$ | -54 mV | |
| | $k_{h,T,1}$ | -5.3 mV | $k_{h,T,2}$ | -5.3 mV | |
| | $k_{m,T}$ | 3.3 mV | $g_T$ | 0.66 nS (5 nS in OVX+E2) | |
| $I_{Ca}$ | $\tau_{h,Ca}$ | 10 ms | $V_{h,Ca}$ | -48.9 | fitted |
| | $\tau_{m,Ca}$ | 300 ms | $V_{m,Ca}$ | -27.3 mV | |
| | $k_{h,Ca}$ | -18.2 | $k_{m,Ca}$ | 4.62 mV | |
| | $g_{Ca}$ | 2.1 nS (2.8 nS in OVX+E2) | $E_{Ca}$ | 121.6 mV | |

**Table S1.** (continued)

| | | | | | |
|---|---|---|---|---|---|
| $I_{TRPC5}$ | $c_{TRPC5}$ | 0.6 μM | $k_{TRPC5}$ | 0.33 μM | [11] |
| | $k_{R_{TRPC5}}$ | 0.006 $ms^{-1}$ | $k_{-R_{TRPC5}}$ | 0.002 $ms^{-1}$ | |
| | $k_{R_{TRPC5},0}$ | 0.002 $ms^{-1}$ | $g_{TRPC5}$ | 8.4 nS (1.68 nS in OVX+E2) | |
| | $K_{NKB}$ | 32 μM | $n2$ | 2 | |
| | $R_{TRPC5,T}$ | 1 μM | $E_{TRPC5}$ | -15 mV | |
| $I_{GIRK}$ | $V_{GIRK}$ | -70 mV | $k_{GIRK,1}$ | 20 mV | [12] |
| | $\alpha$ | 0.8 | $\alpha_\tau$ | 0.0061 | |
| | $k_{GIRK,2}$ | 100 mV | $\beta_\tau$ | 0.0818 | |
| | $g_{GIRK}$ | 0.4 nS | $E_K$ | -81 mV | |
| | $k_{R_{GIRK},0}$ | 0 $ms^{-1}$ | $k_{R_{GIRK}}$ | $10^{-3}$ $ms^{-1}$ | |
| | $R_{GIRK,T}$ | 1 μM | $K_S$ | 1 μM | |
| | $k_{-R_{GIRK}}$ | $3.3 \cdot 10^{-6}$ $ms^{-1}$ | $n3$ | 2 | |
| $I_{leak}$ | | | $g_{leak,2}$ | 3.5 nS in OVX<br>3.65 nS in OVX+E2 | fitted |
| Intracellular calcium | | | | | |
| | $\gamma$ | $1.96 \cdot 10^{-5}$ μM $nA^{-1}$ $ms^{-1}$ | $d_{ca}$ | 0.008 $ms^{-1}$ | [6] |

[1] Parameters *g*. denote the maximum conductance associated with each current.

**Table S1.** (continued)

# References


Ambudkar IS, Ong HL (2007) **Organization and function of TRPC channelsomes** *Pflügers Archiv: European Journal of Physiology* **455**:187–200 https://doi.org/10.1007/s00424-007-0252-0

Andrade R, Foehring R, Tzingounis A. (2012) **The calcium-activated slow AHP: cutting through the Gordian knot** *Frontiers in Cellular Neuroscience* **6** https://doi.org/10.3389/fncel.2012.00047

Biosystems Applied (2006) **Amplification efficiency of TaqMan Gene Expression Assays**

Arboit A, Reboreda A, Yoshida M. (2020) **Involvement of TRPC4 and 5 Channels in Persistent Firing in Hippocampal CA1 Pyramidal Cells** *Cells* **9** https://doi.org/10.3390/cells9020365

Bal T, McCormick DA (1993) **Mechanisms of oscillatory activity in guinea-pig nucleus reticularis thalami in vitro: a mammalian pacemaker** *The Journal of Physiology* **468**:669–691 https://doi.org/10.1113/jphysiol.1993.sp019794

Bengtson CP, Tozzi A, Bernardi G, Mercuri NB (2004) **Transient receptor potential-like channels mediate metabotropic glutamate receptor EPSCs in rat dopamine neurones** *The Journal of Physiology* **555**:323–330 https://doi.org/10.1113/jphysiol.2003.060061

Berg AP, Sen N, Bayliss DA (2007) **TrpC3/C7 and Slo2.1 are molecular targets for metabotropic glutamate receptor signaling in rat striatal cholinergic interneurons** *The Journal of Neuroscience* **27**:8845–8856 https://doi.org/10.1523/JNEUROSCI.0551-07.2007

Birnbaumer L. (2009) **The TRPC class of ion channels: a critical review of their roles in slow, sustained increases in intracellular Ca2+ concentrations** *Annual Review of Pharmacology and Toxicology* **49**:395–426 https://doi.org/10.1146/annurev.pharmtox.48.113006.094928

Blair NT, Kaczmarek JS, Clapham DE (2009) **Intracellular calcium strongly potentiates agonist-activated TRPC5 channels** *The Journal of General Physiology* **133**:525–546 https://doi.org/10.1085/jgp.200810153

Blatz AL, Magleby KL (1987) **Calcium-activated potassium channels** *Trends in Neurosciences* **10**:463–467 https://doi.org/10.1016/0166-2236(87)90101-9

Blum T, Moreno-Pérez A, Pyrski M, Bufe B, Arifovic A, Weissgerber P, Freichel M, Zufall F, Leinders-Zufall T. (2019) **Trpc5 deficiency causes hypoprolactinemia and altered function of oscillatory dopamine neurons in the arcuate nucleus** *Proceedings of the National Academy of Sciences* **116**:15236–15243 https://doi.org/10.1073/pnas.1905705116

Bond CT, Herson PS, Strassmaier T, Hammond R, Stackman R, Maylie J, Adelman JP (2004) **Small conductance Ca2+-activated K+ channel knock-out mice reveal the identity of calcium-dependent afterhyperpolarization currents** *The Journal of Neuroscience* **24**:5301–5306 https://doi.org/10.1523/JNEUROSCI.0182-04.2004

Bond CT, Maylie J, Adelman JP (1999) **Small-conductance calcium-activated potassium channels** *Annals of the New York Academy of Sciences* **868**:370–378 https://doi.org/10.1111/j.1749-6632.1999.tb11298.x

Bond CT, Maylie J, Adelman JP (2005) **SK channels in excitability, pacemaking and synaptic integration** *Current Opinion in Neurobiology* **15**:305–311 https://doi.org/10.1016/j.conb.2005.05.001

Bosch MA, Kelly MJ, Rønnekleiv OK (2002) **Distribution, neuronal co-localization and 17β-E2 modulation of small conductance calcium-activated K+ channel (SK3) mRNA in the guinea pig brain** *Endocrinology* **143**:1097–1107 https://doi.org/10.1210/endo.143.3.8708

Bosch MA, Tonsfeldt KJ, Rønnekleiv OK (2013) **mRNA expression of ion channels in GnRH neurons: subtype-specific regulation by 17β-Estradiol** *Molecular and Cellular Endocrinology* **367**:85–97 https://doi.org/10.1016/j.mce.2012.12.021

Brereton MF, Wareing M, Jones RL, Greenwood SL (2013) **Characterisation of K+ Channels in Human Fetoplacental Vascular Smooth Muscle Cells** *PLOS One* **8** https://doi.org/10.1371/journal.pone.0057451

Brown DA, Passmore GM (2009) **Neural KCNQ (Kv7) channels** *British Journal of Pharmacology* **156**:1185–1195 https://doi.org/10.1111/j.1476-5381.2009.00111.x

Clapham DE (2003) **TRP channels as cellular sensors** *Nature* **426**:517–524 https://doi.org/10.1038/nature02196

Conde K, Roepke T. (2019) **17β-estradiol increases arcuate KNDy neuronal sensitivity to ghrelin inhibition of the M-current in female mice** *Neuroendocrinology* https://doi.org/10.1159/000503146

d'Anglemont de Tassigny X, Fagg LA, Carlton MB, Colledge WH (2008) **Kisspeptin can stimulate gonadotropin-releasing hormone (GnRH) release by a direct action at GnRH nerve terminals** *Endocrinology* **149**:3926–3932 https://doi.org/10.1210/en.2007-1487

De Roux N, Genin E, Carel J-C, Matsuda F, Chaussain J-L, Milgrom E. (2003) **Hypogonadotropic hypogonadism due to loss of function of the KiSS 1-derived peptide receptor GPR54** *Proceedings of the National Academy of Sciences USA* **100**:10972–10976 https://doi.org/10.1073/pnas.1834399100

Erickson KR, Rønnekleiv OK, Kelly MJ (1993) **Electrophysiology of guinea-pig supraoptic neurones: role of a hyperpolarization-activated cation current in phasic firing** *The Journal of Physiology* **460**:407–425 https://doi.org/10.1113/jphysiol.1993.sp019478

Erickson KR, Rønnekleiv OK, Kelly MJ (1993) **Role of a T-type calcium current in supporting a depolarizing potential, damped oscillations, and phasic firing in vasopressinergic guinea pig supraoptic neurons** *Neuroendocrinology* **57**:789–800 https://doi.org/10.1159/000126438

Evans NP, Dahl GE, Mauger D, Karsch FJ (1995) **Estradiol induces both qualitative and quantitative changes in the pattern of gonadotropin-releasing hormone secretion during the presurge period in the ewe** *Endocrinology* **136**:1603–1609 https://doi.org/10.1210/endo.136.4.7895670

Evans NP, Dahl GE, Mauger DT, Padmanabhan V, Thrun LA, Karsch FJ (1995) **Does estradiol induce the preovulatory gonadotropin-releasing hormone (GnRH) surge in the ewe by inducing a progressive change in the mode of operation of the GnRH neurosecretory system** *Endocrinology* **136**:5511–5519 https://doi.org/10.1210/endo.136.12.7588302

Faber ES, Sedlak P, Vidovic M, Sah P. (2006) **Synaptic activation of transient receptor potential channels by metabotropic glutamate receptors in the lateral amygdala** *Neuroscience* **137**:781–794 https://doi.org/10.1016/j.neuroscience.2005.09.027

Goodman RL *et al.* (2007) **Kisspeptin neurons in the arcuate nucleus of the ewe express both dynorphin A and neurokinin B** *Endocrinology* **148**:5752–5760 https://doi.org/10.1210/en.2007-0961

Gore BB, Soden ME, Zweifel LS (2013) **Manipulating gene expression in projection-specific neuronal populations using combinatorial viral approaches** *Current Protocols in Neuroscience* **65**:1–20 https://doi.org/10.1002/0471142301.ns0435s65

Gottsch ML *et al.* (2011) **Molecular properties of Kiss1 neurons in the arcuate nucleus of the mouse** *Endocrinology* **152**:4298–4309 https://doi.org/10.1210/en.2011-1521

Greene DL, Kang S, Hoshi N. (2017) **XE991 and linopirdine are state-dependent inhibitors for Kv7/KCNQ channels that favor activated single subunits** *Journal of Pharmacology and Experimental Therapeutics* **362**:177–185 https://doi.org/10.1124/jpet.117.241679

Gu N, Vervaeke K, Storm JF (2007) **BK potassium channels facilitate high-frequency firing and cause early spike frequency adaptation in rat CA1 hippocampal pyramidal cells** *The Journal of Physiology* **580**:859–882 https://doi.org/10.1113/jphysiol.2006.126367

Han SY, Morris PG, Kim J-C, Guru S, Pardo-Navarro M, Yeo S-H, McQuillan HJ, Herbison AE (2023) **Mechanism of kisspeptin neuron synchronization for pulsatile hormone secretion in male mice** *Cell Reports* **42** https://doi.org/10.1016/j.celrep.2022.111914

Hiraizumi Y, Nishimura I, Ishii H, Tanaka N, Takeshita T, Sakuma Y, Kato M. (2008) **Rat GnRH neurons exhibit large conductance voltage- and Ca2+-Activated K+ (BK) currents and express BK channel mRNAs** *The Journal of Physiological Sciences* **58**:21–29 https://doi.org/10.2170/physiolsci.RP013207

Hodgkin AL, Huxley AF (1952) **A quantitative description of membrane current and its application to conduction and excitation in nerve** *The Journal of Physiology* **117**:500–544 https://doi.org/10.1113/jphysiol.1952.sp004764

Hunker AC, Soden ME, Krayushkina D, Heymann G, Awatramani R, Zweifel LS (2020) **Conditional single vector CRISPR/SaCas9 viruses for efficient mutagenesis in the adult mouse nervous system** *Cell Reports* **30**:4303–4316 https://doi.org/10.1016/j.celrep.2020.02.092

Kato M, Ui-Tei K, Watanabe M, Sakuma Y. (2003) **Characterization of voltage-gated calcium currents in gonadotropin-releasing hormone neurons tagged with green fluorescent protein in rats** *Endocrinology* **144**:5118–5125 https://doi.org/10.1210/en.2003-0213

Kelly MJ, Qiu J, Rønnekleiv OK (2018) **TRPCing around the hypothalamus** *Frontiers in Neuroendocrinology* **51**:116–124 https://doi.org/10.1016/j.yfrne.2018.05.004

Kelly MJ, Rønnekleiv OK, Levine J. E. (1994) **Electrophysiological analysis of neuroendocrine neuronal activity in hypothalamic slices** *Methods in Neurosciences: Pulsatility in Neuroendocrine Systems* :47–67 https://doi.org/10.1016/B978-0-12-185289-4.50009-7

Kotani M *et al.* (2001) **The metastasis suppressor gene KiSS-1 encodes kisspeptins, the natural ligands of the orphan G protein-coupled receptor GPR54** *Journal of Biological Chemistry* **276**:34631–34636 https://doi.org/10.1074/jbc.M104847200

Kshatri AS, Gonzalez-Hernandez A, Giraldez T. (2018) **Physiological roles and therapeutic potential of Ca2+ activated potassium channels in the nervous system** *Frontiers in Molecular Neuroscience* **11** https://doi.org/10.3389/fnmol.2018.00258

Lancaster B, Nicoll RA (1987) **Properties of two calcium-activated hyperpolarizations in rat hippocampal neurones** *The Journal of Physiology* **389**:187–203 https://doi.org/10.1113/jphysiol.1987.sp016653

Lee S-C, Choi S, Lee T, Kim H-L, Chin H, Shin H-S. (2002) **Molecular basis of R-type calcium channels in central amygdala neurons of the mouse** *Proceedings of the National Academy of Sciences* **99**:3276–3281 https://doi.org/10.1073/pnas.052697799

Lehman MN, Hileman SM, Goodman RL (2013) **Neuroanatomy of the kisspeptin signaling system in mammals: comparative and developmental aspects** *Advances in Experimental Medicine and Biology* **784**:27–62 https://doi.org/10.1007/978-1-4614-6199-9_3

Lehman MN, Merkley CM, Coolen LM, Goodman RL (2010) **Anatomy of the kisspeptin neural network in mammals** *Brain Research* **1364**:90–102 https://doi.org/10.1016/j.brainres.2010.09.020

Lin XH, Lass G, Kong LS, Wang H, Li XF, Huang HF, O'Byrne KT (2021) **Optogenetic activation of arcuate kisspeptin neurons generates a luteinizing hormone surge-Like secretion in an estradiol-dependent manner** *Frontiers in Endocrinology* https://doi.org/10.3389/fendo.2021.775233

Liu X, Yeo S-H, McQuillan HJ, Herde MK, Hessler S, Cheong I, Porteous R, Herbison AE (2021) **Highly redundant neuropeptide volume co-transmission underlying episodic activation of the GnRH neuron dendron** *eLife* **10** https://doi.org/10.7554/eLife.62455

Livak KJ, Schmittgen TD (2001) **Analysis of relative gene expression data using real-time quantitative PCR and the 2−ΔΔCT method** *Methods* **25**:402–408 https://doi.org/10.1006/meth.2001.1262

Llinás RR. (1988) **The intrinsic electrophysiological properties of mammalian neurons: insights into central nervous system function** *Science* **242**:1654–1664 https://doi.org/10.1126/science.3059497

Lüthi A, McCormick DA (1998) **H-current: properties of a neuronal and network pacemaker** *Neuron* **21**:9–12 https://doi.org/10.1016/S0896-6273(00)80509-7

Lyons DJ, Hellysaz A, Broberger C. (2012) **Prolactin regulates tuberoinfundibular dopamine neuron discharge pattern: novel feedback control mechanisms in the lactotrophic axis** *The Journal of Neuroscience* **32**:8074–8083 https://doi.org/10.1523/JNEUROSCI.0129-12.2012

Lyons DJ, Horjales-Araujo E, Broberger C. (2010) **Synchronized network oscillations in rat tuberoinfundibular dopamine neurons: swith to tonic discharge by thyrotropin-releasing hormone** *Neuron* **65**:217–229 https://doi.org/10.1016/j.neuron.2009.12.024

Madisen L *et al.* (2012) **A toolbox of Cre-dependent optogenetic transgenic mice for light-induced activation and silencing** *Nature Neuroscience* **15**:793–802 https://doi.org/10.1038/nn.3078

Marrion NV, Tavalin SJ (1998) **Selective activation of Ca2+-activated K+ channels by co-localize Ca2+ channels in hippocampal neurons** *Nature* **395**:900–905 https://doi.org/10.1038/27674

Marty A. (1989) **The physiological role of calcium-dependent channels** *Trends in Neurosciences* **12**:420–424 https://doi.org/10.1016/0166-2236(89)90090-8

McNally BA, Plante AE, Meredith AL (2020) **Diurnal properties of voltage-gated Ca2+ currents in suprachiasmatic nucleus and roles in action potential firing** *The Journal of Physiology* **598**:1775–1790 https://doi.org/10.1113/JP278327

Mendonça PRF, Kyle V, Yeo SH, Colledge WH, Robinson HPC (2018) **Kv4.2 channel activity controls intrinsic firing dynamics of arcuate kisspeptin neurons** *The Journal of Physiology* **596**:885–899 https://doi.org/10.1113/JP274474

Messager S *et al.* (2005) **Kisspeptin directly stimulates gonadotropin-releasing hormone release via G protein-coupled receptor 54** *Proceedings of the National Academy of Sciences USA* **102**:1761–1766 https://doi.org/10.1073/pnas.0409330102

Moenter SM, Caraty A, Lehman MN, Karsch FJ (1993) **Characterization and regulation of pre-ovulatory secretion of gonadotrophin-releasing hormone** *Human Reproduction 8 Suppl* **2**:51–56 https://doi.org/10.1093/humrep/8.suppl_2.51

Navarro VM, Gottsch ML, Chavkin C, Okamura H, Clifton DK, Steiner RA (2009) **Regulation of gonadotropin-releasing hormone secretion by kisspeptin/dynorphin/neurokinin B neurons in the arcuate nucleus of the mouse** *The Journal of Neuroscience* **29**:11859–11866 https://doi.org/10.1523/JNEUROSCI.1569-09.2009

Navarro VM *et al.* (2011) **Regulation of NKB pathways and their roles in the control of Kiss1 neurons in the arcuate nucleus of the male mouse** *Endocrinology* **152**:4265–4275 https://doi.org/10.1210/en.2011-1143

Nestor CC, Qiu J, Padilla SL, Zhang C, Bosch MA, Fan W, Aicher SA, Palmiter RD, Rønnekleiv OK, Kelly MJ (2016) **Optogenetic stimulation of arcuate nucleus Kiss1 neurons reveals a steroid-dependent glutamatergic input to POMC and AgRP neurons in male mice** *Molecular Endocrinology* **30**:630–644 https://doi.org/10.1210/me.2016-1026

Nicoll RA (1988) **The coupling of neurotransmitter receptors to ion channels in the brain** *Science* **241**:545–551 https://doi.org/10.1126/science.2456612

Niday Z, Bean BP (2021) **BK channel regulation of afterpotentials and burst firing in Cerebellar Purkinje neurons** *The Journal of Neuroscience* **41**:2854–2869 https://doi.org/10.1523/jneurosci.0192-20.2021

Nunemaker CS, DeFazio RA, Moenter SM (2003) **Calcium current subtypes in GnRH neurons** *Biology of Reproduction* **69**:1914–1922 https://doi.org/10.1095/biolreprod.103.019265

O'Byrne KT, Thalabard JC, Grosser PM, Wilson RC, Williams CL, Chen MD, Ladendorf D, Hotchkiss J, Knobil E. (1991) **Radiotelemetric monitoring of hypothalamic gonadotropin-releasing hormone pulse generator activity throughout the menstrual cycle of the rhesus monkey** *Endocrinology* **129**:1207–1214 https://doi.org/10.1210/endo-129-3-1207

Padilla SL, Johnson CW, Barker FD, Patterson MA, Palmiter RD (2018) **A neural circuit underlying the generation of hot flushes** *Cell Reports* **24**:271–277 https://doi.org/10.1016/j.celrep.2018.06.037

Perez-Reyes E. (2003) **Molecular physiology of low-voltage-activated t-type calcium channels** *Physiological Reviews* **83**:117–161 https://doi.org/10.1152/physrev.00018.2002

Peters HC, Hu H, Pongs O, Storm JF, Isbrandt D. (2005) **Conditional transgenic suppression of M channels in mouse brain reveals functions in neuronal excitability, resonance and behavior** *Nature Neuroscience* **8**:51–60 https://doi.org/10.1038/nn1375

Pfaffl MW (2001) **A new mathematical model for relative quantification in real-time RT-PCR** *Nucleic Acids Research* **29** https://doi.org/10.1093/nar/29.9.e45

Qiu J, Bosch MA, Jamali K, Xue C, Kelly MJ, Rønnekleiv OK (2006) **Estrogen upregulates T-type calcium channels in the hypothalamus and pituitary** *The Journal of Neuroscience* **26**:11072–11082 https://doi.org/10.1523/JNEUROSCI.3229-06.2006

Qiu J, Bosch MA, Tobias SC, Grandy DK, Scanlan TS, Rønnekleiv OK, Kelly MJ (2003) **Rapid signaling of estrogen in hypothalamic neurons involves a novel G-protein-coupled estrogen receptor that activates protein kinase C** *The Journal of Neuroscience* **23**:9529–9540 https://doi.org/10.1523/JNEUROSCI.23-29-09529.2003

Qiu J, Fang Y, Rønnekleiv OK, Kelly MJ (2010) **Leptin excites proopiomelanocortin neurons via activation of TRPC channels** *The Journal of Neuroscience* **30**:1560–1565 https://doi.org/10.1523/JNEUROSCI.4816-09.2010

Qiu J, Nestor CC, Zhang C, Padilla SL, Palmiter RD, Kelly MJ, Rønnekleiv OK (2016) **High-frequency stimulation-induced peptide release synchronizes arcuate kisspeptin neurons and excited GnRH neurons** *eLife* **5** https://doi.org/10.7554/eLife.16246

Qiu J, Rivera HM, Bosch MA, Padilla SL, Stincic TL, Palmiter RD, Kelly MJ, Rønnekleiv OK (2018) **Estrogenic-dependent glutamatergic neurotransmission from kisspeptin neurons governs feeding circuits in females** *eLife* **7** https://doi.org/10.7554/eLife.35656

Qiu J, Stincic TL, Bosch MA, Connors AM, Petrie SK, Rønnekleiv OK, Kelly MJ (2021) **Deletion of Stim1 in hypothalamic arcuate nucleus Kiss1 neurons potentiates synchronous GCaMP activity and protects against diet-induced obesity** *J Neurosc* **41**:9688–9701 https://doi.org/10.1523/JNEUROSCI.0622-21.2021

Qiu J, Zhang C, Borgquist A, Nestor CC, Smith AW, Bosch MA, Ku S, Wagner EJ, Rønnekleiv OK, Kelly MJ (2014) **Insulin excites anorexigenic proopiomelanocortin neurons via activation of canonical transient receptor potential channels** *Cell Metabolism* **19**:682–693 https://doi.org/10.1016/j.cmet.2014.03.004

Rance NE (2009) **Menopause and the human hypothalamus: Evidence for the role of kisspeptin/neurokinin B neurons in the regulation of esstrogen negative feedback** *Peptides* **30**:111–122 https://doi.org/10.1016/j.peptides.2008.05.016

Rance NE, Young WS (1991) **Hypertrophy and increased gene expression of neurons containing neurokinin-B and substance-P messenger ribonucleic acids in the hypothalami of postmenopausal women** *Endocrinology* **128**:2239–2247 https://doi.org/10.1210/endo-128-5-2239

Roepke TA, Qiu J, Smith AW, Rønnekleiv OK, Kelly MJ (2011) **Fasting and 17β-estradiol differentially modulate the M-current in neuropeptide Y neurons** *The Journal of Neuroscience* **17**:11825–11835 https://doi.org/10.1523/JNEUROSCI.1395-11.2011

Rønnekleiv OK, Qiu J, Kelly MJ (2022) **Hypothalamic kisspeptin neurons and the control of homeostasis** *Endocrinology* **163**:1–11 https://doi.org/10.1210/endocr/bqab253

Rossmanith WG, Liu CH, Laughlin GA, Mortola JF, Suh BY, Yen SSC (1990) **Relative changes in LH pulsatility during the menstrual cycle: Using data from hypogonadal women as a reference point** *Clinical Endocrinology* **32**:647–660 https://doi.org/10.1111/j.1365-2265.1990.tb00909.x

Sah P. (1996) **Ca2+-activated K+ currents in neurones: Types, physiological roles and modulation** *Trends in Neurosciences* **19**:150–154 https://doi.org/10.1016/s0166-2236(96)80026-9

Sah P, Clements JD (1999) **Photolytic manipulation of [Ca2+]i reveals slow kinetics of potassium channels underlying the afterhyperpolarization in hippocampal pyramidal neurons** *The Journal of Neuroscience* **19**:3657–3664 https://doi.org/10.1523/JNEUROSCI.19-10-03657

Sah P, Louise Faber ES (2002) **Channels underlying neuronal calcium-activated potassium currents** *Progress in Neurobiology* **66**:345–353 https://doi.org/10.1016/S0301-0082(02)00004-7

Schmittgen TD, Livak KJ (2008) **Analyzing real-time PCR data by the comparative CT method** *Nature Protocols* **3**:1101–1108 https://doi.org/10.1038/nprot.2008.73

Seminara SB *et al.* (2003) **The GPR54 gene as a regulator of puberty** *The New England Journal of Medicine* **349**:1614–1627 https://doi.org/10.1056/NEJMoa035322

Shahab M, Mastronardi C, Seminara SB, Crowley WF, Ojeda SR, Plant TM (2005) **Increased hypothalamic GPR54 signaling: a potential mechanism for initiation of puberty in primates** *Proceedings of the National Academy of Sciences of the United States of America* **102**:2129–2134 https://doi.org/10.1073/pnas.0409822102

Shao LR, Halvorsrud R, Borg-Graham L, Storm JF (1999) **The role of BK-type Ca2+-dependent K+ channels in spike broadening during repetitive firing in rat hippocampal pyramidal cells** *The Journal of Physiology* **521**:135–146 https://doi.org/10.1111/j.1469-7793.1999.00135.x

Smith JT, Cunningham MJ, Rissman EF, Clifton DK, Steiner RA (2005) **Regulation of Kiss1 gene expression in the brain of the female mouse** *Endocrinology* **146**:3686–3692 https://doi.org/10.1210/en.2005-0488

Spergel DJ (2007) **Calcium and small-conductance calcium-activated potassium channels in gonadotropin-releasing hormone neurons before, during, and after puberty** *Endocrinology* **148**:2383–2390 https://doi.org/10.1210/en.2006-1693

Stincic TL, Bosch MA, Hunker AC, Juarez B, Connors AM, Zweifel LS, Rønnekleiv OK, Kelly MJ (2021) **CRISPR knockdown of Kcnq3 attenuates the M current and increases excitability of NPY/AgRP neurons to alter energy balance** *Molecular Metabolism* https://doi.org/10.1016/j.molmet.2021.101218

Storm JF (1987) **Action potential repolarization and a fast after-hyperpolarization in rat hippocampal pyramidal cells** *The Journal of Physiology* **385**:733–759

Storm JF (1990) **Potassium currents in hippocampal pyramidal cells** *Progress in Brain Research* **83**:161–187 https://doi.org/10.1016/s0079-6123(08)61248-0

Tian J-b, Yang J, Joslin WC, Flockerzi V, Prescott SA, Birnbaumer L, Zhu MX (2022) **TRPC4 and GIRK channels underlie neuronal coding of firing patterns that reflect Gq/11 -Gi/o coincidence signals of variable strengths** *Proceedings of the National Academy of Sciences* **119** https://doi.org/10.1073/pnas.2120870119

Tozzi A, Bengtson CP, Longone P, Carignani C, Fusco FR, Bernardi G, Mercuri NB (2003) **Involvement of transient receptor potential-like channels in responses to mGluR-I activation in midbrain dopamine neurons** *European Journal of Neuroscience* **18**:2133–2145 https://doi.org/10.1046/j.1460-9568.2003.02936.x

Tsien RW, Hess P, McCleskey EW, Rosenberg RL (1987) **Calcium channels: mechanisms of selectivity, permeation, and block** *Annual Review of Biophysics and Biophysical Chemistry* **16**:265–290 https://doi.org/10.1146/annurev.bb.16.060187.001405

Tzingounis AV, Heidenreich M, Kharkovets T, Spitzmaul G, Jensen HS, Nicoll RA, Jentsch TJ (2010) **The KCNQ5 potassium channel mediates a component of the afterhyperpolarization current in mouse hippocampus** *Proceedings of the National Academy of Sciences of the United States of America* **107**:10232–10237 https://doi.org/10.1073/pnas.1004644107

Tzingounis AV, Kobayashi M, Takamatsu K, Nicoll RA (2007) **Hippocalcin gates the calcium activation of the slow afterhyperpolarization in hippocampal pyramidal cellls** *Neuron* **53**:487–493 https://doi.org/10.1016/j.neuron.2007.01.011

Tzingounis AV, Nicoll RA (2008) **Contribution of KCNQ2 and KCNQ3 to the medium and slow afterhyperpolarization currents** *Proceedings of the National Academy of Sciences of the United States of America* **105**:19974–19979 https://doi.org/10.1073/pnas.0810535105

Venkatachalam K, Montell C. (2007) **TRP channels** *Annual Review of Biochemistry* **76**:387–417 https://doi.org/10.1146/annurev.biochem.75.103004.142819

Vogalis F, Storm JF, Lancaster B. (2003) **SK channels and the varieties of slow after-hyperpolarizations in neurons** *European Journal of Neuroscience* **18**:3155–3166 https://doi.org/10.1111/j.1460-9568.2003.03040.x

Voliotis M, Li XF, De Burgh RA, Lass G, Ivanova D, McIntyre C, O'Byrne K, Tsaneva-Atanasova K. (2021) **Modulation of pulsatile GnRH dynamics across the ovarian cycle via changes in the network excitability and basal activity of the arcuate kisspeptin network** *eLife* **10** https://doi.org/10.7554/eLife.71252

Wakabayashi Y *et al.* (2010) **Neurokinin B and dynorphin A in kisspeptin neurons of the arcuate nucleus participate in generation of periodic oscillation of neural activity driving pulsatile gonadotropin-releasing hormone secretion in the goat** *The Journal of Neuroscience* **30**:3124–3132 https://doi.org/10.1523/JNEUROSCI.5848-09.2010

Whorton MR, MacKinnon R. (2011) **Crystal structure of the mammalian GIRK2 K+ channel and gating regulation by G proteins, PIP2, and sodium** *Cell* **147**:199–208 https://doi.org/10.1016/j.cell.2011.07.046

Zagotta WN, Siegelbaum SA (1996) **Structure and function of cyclic nucleotide-gated channels** *Annual Review of Neuroscience* **19**:235–263 https://doi.org/10.1146/annurev.ne.19.030196.001315

Zhang C, Bosch MA, Rick EA, Kelly MJ, Rønnekleiv OK (2009) **17β-estradiol regulation of T-type calcium channels in gonadotropin-releasing hormone neurons** *The Journal of Neuroscience* **29**:10552–10562 https://doi.org/10.1523/JNEUROSCI.2962-09.2009

Zhang C, Rønnekleiv OK, Kelly MJ (2013) **Kisspeptin inhibits a slow afterhyperpolarization current via protein kinase C and reduces spike frequency adaptation in GnRH neurons** *American Journal of Physiology: Endocrinology and Metabolism* **304**:E1237–1244 https://doi.org/10.1152/ajpendo.00058.2013

Zhang XB, Spergel DJ (2012) **Kisspeptin inhibits high-voltage activated Ca2+ channels in GnRH neurons via multiple Ca2+ influx and release pathways** *Neuroendocrinology* **96**:68–80 https://doi.org/10.1159/000335985

Zhang Z, Reboreda A, Alonso A, Barker PA, Séguéla P. (2011) **TRPC channels underlie cholinergic plateau potentials and persistent activity in entorhinal cortex** *Hippocampus* **21**:386–397 https://doi.org/10.1002/hipo.20755

Zheng Y, Liu H, Chen Y, Dong S, Wang F, Wang S, Li G-L, Shu Y, Xu F. (2022) **Structural insights into the lipid and ligand regulation of a human neuronal KCNQ channel** *Neuron* **110**:237–247 https://doi.org/10.1016/j.neuron.2021.10.029

Zylberberg J, Strowbridge BW (2017) **Mechanisms of Persistent Activity in Cortical Circuits: Possible Neural Substrates for Working Memory** *Annual Review of Neuroscience* **40**:603–627 https://doi.org/10.1146/annurev-neuro-070815-014006

1. Fry M., Boegle A.K., Maue R.A. (2007) **Differentiated pattern of sodium channel expression in dissociated Purkinje neurons maintained in long-term culture** *J Neurochem* **101**:737–48

2. Zhang C., et al. (2015) **17beta-Estradiol increases persistent Na(+) current and excitability of AVPV/PeN Kiss1 neurons in female mice** *Mol Endocrinol* **29**:518–27

3. Moran S., Moenter S.M., Khadra A. (2016) **A unified model for two modes of bursting in GnRH neurons** *J Comput Neurosci* **40**:297–315

4. Mendonca P.R., et al. (2016) **Stochastic and deterministic dynamics of intrinsically irregular firing in cortical inhibitory interneurons** *Elife* **5**

5. Mendonca P.R.F., et al. (2018) **Kv4.2 channel activity controls intrinsic firing dynamics of arcuate kisspeptin neurons** *J Physiol* **596**:885–899

6. Tsaneva-Atanasova K., et al. (2007) **Mechanism of spontaneous and receptor-controlled electrical activity in pituitary somatotrophs: experiments and theory** *J Neurophysiol* **98**:131–44

7. Booth C.A., et al. (2016) **Altered Intrinsic Pyramidal Neuron Properties and Pathway-Specific Synaptic Dysfunction Underlie Aberrant Hippocampal Network Function in a Mouse Model of Tauopathy** *J Neurosci* **36**:350–63

8. Conde K., Roepke T.A. (2020) **17beta-Estradiol Increases Arcuate KNDy Neuronal Sensitivity to Ghrelin Inhibition of the M-Current in Female Mice** *Neuroendocrinology* **110**:582–594

9. Nowacki J., et al. (2011) **A unified model of CA1/3 pyramidal cells: an investigation into excitability** *Prog Biophys Mol Biol* **105**:34–48

10. Wang L., DeFazio R.A., Moenter S.M. (2016) **Excitability and Burst Generation of AVPV Kisspeptin Neurons Are Regulated by the Estrous Cycle Via Multiple Conductances Modulated by Estradiol Action** *eNeuro* **3**

11. Qiu J., et al. (2021) **Deletion of Stim1 in Hypothalamic Arcuate Nucleus Kiss1 Neurons Potentiates Synchronous GCaMP Activity and Protects against Diet-Induced Obesity** *J Neurosci* **41**:9688–9701

12. Tian J.B., et al. (2022) **TRPC4 and GIRK channels underlie neuronal coding of firing patterns that reflect G(q/11)-G(i/o) coincidence signals of variable strengths** *Proc Natl Acad Sci U S A* **119**

13. Bond C.T., Maylie J., Adelman J.P. (1999) **Small-conductance calcium-activated potassium channels** *Ann N Y Acad Sci* **868**:370–8

14. Gottsch M.L., et al. (2011) **Molecular properties of Kiss1 neurons in the arcuate nucleus of the mouse** *Endocrinology* **152**:4298–309

15. Qiu J., et al. (2018) **Estrogenic-dependent glutamatergic neurotransmission from kisspeptin neurons governs feeding circuits in females** *Elife* **7**

## Article and author information

**Jian Qiu**
Department of Chemical Physiology and Biochemistry, Oregon Health & Science U., Portland, OR 97239, USA
**For correspondence:** qiuj@ohsu.edu;
ORCID iD: 0000-0002-4988-8587

**Margaritis Voliotis**
Department of Mathematics and Statistics, University of Exeter, Stocker Rd, Exeter, EX4 4PY, UK, Living Systems Institute, University of Exeter, Stocker Rd, Exeter, EX4 4PY, UK
ORCID iD: 0000-0001-6488-7198

**Martha A. Bosch**
Department of Chemical Physiology and Biochemistry, Oregon Health & Science U., Portland, OR 97239, USA

**Xiao Feng Li**
Department of Women and Children's Health, School of Life Course and Population Sciences, King's College London, Guy's Campus, London SE1 1UL, UK

**Larry S. Zweifel**
Department of Psychiatry and Behavioral Sciences, University of Washington, Seattle, WA 98195, USA, Depatment of Pharmacology, University of Washington, Seattle, WA 98195, USA
ORCID iD: 0000-0003-3465-5331

**Krasimira Tsaneva-Atanasova**
Department of Mathematics and Statistics, University of Exeter, Stocker Rd, Exeter, EX4 4PY, UK, Living Systems Institute, University of Exeter, Stocker Rd, Exeter, EX4 4PY, UK
ORCID iD: 0000-0002-6294-7051

**Kevin T. O'Byrne**
Department of Women and Children's Health, School of Life Course and Population Sciences, King's College London, Guy's Campus, London SE1 1UL, UK
ORCID iD: 0000-0002-2548-4182

**Oline K. Rønnekleiv**
Department of Chemical Physiology and Biochemistry, Oregon Health & Science U., Portland, OR 97239, USA, Division of Neuroscience, Oregon National Primate Research Center, Beaverton, OR 97006, USA
ORCID iD: 0000-0003-1841-4386

**Martin J. Kelly**
Department of Chemical Physiology and Biochemistry, Oregon Health & Science U., Portland, OR 97239, USA, Division of Neuroscience, Oregon National Primate Research Center, Beaverton, OR 97006, USA
**For correspondence:** kellym@ohsu.edu
ORCID iD: 0000-0002-8633-2510

## Copyright

© 2024, Qiu et al.

This article is distributed under the terms of the Creative Commons Attribution License, which permits unrestricted use and redistribution provided that the original author and source are credited.

## Editors

Reviewing Editor
**Helen Scharfman**
Nathan Kline Institute and New York University Langone Medical Center, Orangeburg, United States of America

Senior Editor
**Wei Yan**
The Lundquist Institute, Torrance, United States of America

**Reviewer #1 (Public Review):**

Summary:

In this work, Qiu and colleagues examined the effects of preovulatory (i.e., proestrous or late follicular phase) levels of circulating estradiol on multiple calcium and potassium channel conductances in arcuate nucleus kisspeptin neurons. Although these cells are strongly linked to a role as the "GnRH pulse generator," the goal here was to examine the physiological properties of these cells in a hormonal milieu mimicking late proestrus, the time of the preovulatory GnRH-LH surge. Computational modeling is used to manipulate multiple conductances simultaneously and support a role for certain calcium channels in facilitating a switch in firing mode from tonic to bursting. CRISPR knockdown of the TRPC5 channel reduced overall excitability, but this was only examined in cells from ovariectomized mice without estradiol treatment. The patch clamp experiments are comprehensive and overall solid but a direct demonstration of the role of these conductances in being necessary for

surge generation (or at least having a direct physiological consequence on surge properties) is lacking, substantially reducing the impact of the findings.

Strengths:

(1) Examination of multiple types of calcium and potassium currents, both through electrophysiology and molecular biology.

(2) Focus on arcuate kisspeptin neurons during the surge is relatively conceptually novel as the anteroventral periventricular nucleus (AVPV) kisspeptin neurons have received much more attention as the "surge generator" population.

(3) The modeling studies allow for direct examination of manipulation of single and multiple conductances, whereas the electrophysiology studies necessarily require examination of each current in isolation. The construction of an arcuate kisspeptin neuron model promises to be of value to the reproductive neuroendocrinology field.

Weaknesses:

(1) The novelty of some of the experiments needs to be clarified. This reviewer's understanding is that prior experiments largely used a different OVX+E2 treatment paradigm mimicking periods of low estradiol levels, whereas the present work used a "high E2" treatment model. However, Figures 10C and D are repeated from a previous publication by the same group, according to the figure legend. Findings from "high" vs. "low" E2 treatment regimens should be labeled and clearly separated in the text. It would also help to have direct comparisons between results from low E2 and high E2 treatment conditions.

(2) In multiple places, links are made between the changes in conductances and the transition from peptidergic to glutamatergic neurotransmission. However, this relationship is never directly assessed. The data that come closest are the qPCR results showing reduced Tac2 and increased Vglut2 mRNA, but in the figure legend, it appears that these results are from a prior publication using a different E2 treatment regimen.

(3) Similarly, no recordings of arcuate-AVPV glutamatergic transmission are made so the statements that Kiss1ARH neurons facilitate the GnRH surge via this connection are still only conjecture and not supported by the present experiments.

(4) Figure 1 is not described in the Results section, and is only tenuously connected to the statement in the introduction in which it is cited. The relevance of panels C and D is not clear. In this regard, much is made of the burst firing pattern that arises after E2 treatment in the model, but this burst firing pattern is not demonstrated directly in the slice electrophysiology examples.

(5) In Figure 3, it would be preferable to see the raw values for R1 and R2 in each cell, to confirm that all cells were starting from a similar baseline. In addition, it is unclear why the data for TTA-P2 is not shown, or how many cells were recorded to provide this finding.

(6) In Figure 5, panel C lists 11 cells in the E2 condition but panel E lists data from 37 cells. The reason for this discrepancy is not clear.

(7) In all histogram figures, it would be preferable to have the data for individual cells superimposed on the mean and SEM.

(8) The CRISPR experiments were only performed in OVX mice, substantially limiting interpretation with respect to potential roles for TRPC5 in shaping arcuate kisspeptin neuron function during the preovulatory surge.

(9) Furthermore, there are no demonstrations that the CRISPR manipulations impair or alter the LH surge.

(10) The time of day of slice preparation and recording needs to be specified in the Methods.

https://doi.org/10.7554/eLife.96691.1.sa1

**Reviewer #2 (Public Review):**

Summary:

Kisspeptin neurons of the arcuate nucleus (ARC) are thought to be responsible for the pulsatile GnRH secretory pattern and to mediate feedback regulation of GnRH secretion by estradiol (E2). Evidence in the literature, including the work of the authors, indicates that ARC kisspeptin coordinate their activity through reciprocal synaptic interactions and the release of glutamate and of neuropeptide neurokinin B (NKB), which they co-express. The authors show here that E2 regulates the expression of genes encoding different voltage-dependent calcium channels, calcium-dependent potassium channels, and canonical transient receptor potential (TRPC5) channels and of the corresponding ionic currents in ARC kisspeptin neurons. Using computer simulations of the electrical activity of ARC kisspeptin neurons, the authors also provide evidence of what these changes translate into in terms of these cells' firing patterns. The experiments reveal that E2 upregulates various voltage-gated calcium currents as well as 2 subtypes of calcium-dependent potassium currents while decreasing TRPC5 expression (an ion channel downstream of NKB receptor activation), the slow excitatory synaptic potentials (slow EPSP) elicited in ARC kisspeptin neurons by NKB release and expression of the G protein-associated inward-rectifying potassium channel (GIRK). Based on these results, and on those of computer simulations, the authors propose that E2 promotes a functional transition of ARC kisspeptin neurons from neuropeptide-mediated sustained firing that supports coordinated activity for pulsatile GnRH secretion to a less intense firing in glutamatergic burst-like firing pattern that could favor glutamate release from ARC kisspeptin. The authors suggest that the latter might be important for the generation of the preovulatory surge in females.

Strengths:

The authors combined multiple approaches in vitro and in silico to gain insights into the impact of E2 on the electrical activity of ARC kisspeptin neurons. These include patch-clamp electrophysiology combined with selective optogenetic stimulation of ARC kisspeptin neurons, reverse transcriptase quantitative PCR, pharmacology, and CRIPR-Cas9-mediated knockdown of the Trpc5 gene. The addition of computer simulations for understanding the impact of E2 on the electrical activity of ARC kisspeptin cells is also a strength.

The authors add interesting information on the complement of ionic currents in ARC kisspeptin neurons and on their regulation by E2 to what was already known in the literature. Pharmacological and electrophysiological experiments appear of the highest standards. Robust statistical analyses are provided throughout, although some experiments (illustrated in Figures 7 and 8) do have rather low sample numbers.

The impact of E2 on calcium and potassium currents is compelling. Likewise, the results of Trpc5 gene knockdown do provide good evidence that the TRPC5 channel plays a key role in mediating the NKB-mediated slow EPSP. Surprisingly, this also revealed an unsuspected role for this channel in regulating the membrane potential and excitability of ARC kisspeptin neurons.

Weaknesses:

The manuscript also has weaknesses that obscure some of the conclusions drawn by the authors.

One has to do with the fact that "burst-like" firing that the authors postulate ARC kisspeptin neurons transition to after E2 replacement is only seen in computer simulations, and not in slice patch-clamp recordings. A more direct demonstration of the existence of this firing pattern, and of its prominence over neuropeptide-dependent sustained firing under conditions of high E2 would make a more convincing case for the authors' hypothesis.

In addition, and quite importantly, the authors compare here two conditions, OVX versus OVX replaced with high E2, that may not reflect the physiological conditions (the diestrous [low E2] and proestrous [high E2] stages of the estrous cycle) under which the proposed transition between neuropeptide-dependent sustained firing and less intense burst firing might take place. This is an important caveat to keep in mind when interpreting the authors' findings. Indeed, that E2 alters certain ionic currents when added back to OVX females, does not mean that the magnitude of these ionic currents will vary during the estrous cycle.

Lastly, the results of some of the pharmacological and genetic experiments may be difficult to interpret as presented. For example, in Figure 3, although it is possible that blockade of individual calcium channel subtypes suppresses the slow EPSP through decreased calcium entry at the somato-dendritic compartment to sustain TRPC5 activation and the slow depolarization (as the authors imply), a reasonable alternative interpretation would be that at least some of the effects on the amplitude of the slow EPSP result from suppression of presynaptic calcium influx and, thus, decreased neurotransmitter and neuropeptide secretion. Along the same lines, in Figure 12, one possible interpretation of the observed smaller slow EPSPs seen in mice with mutant TRPC5 could be that at least some of the effect is due to decreased neurotransmitter and neuropeptide release due to the decreased excitability associated with TRPC5 knockdown.

https://doi.org/10.7554/eLife.96691.1.sa0

**Author response:**

> ***Public Reviews:***
>
> ***Reviewer #1 (Public Review):***
>
> *Summary:*
>
> *In this work, Qiu and colleagues examined the effects of preovulatory (i.e., proestrous or late follicular phase) levels of circulating estradiol on multiple calcium and potassium channel conductances in arcuate nucleus kisspeptin neurons. Although these cells are strongly linked to a role as the "GnRH pulse generator," the goal here was to examine the physiological properties of these cells in a hormonal milieu mimicking late proestrus, the time of the preovulatory GnRH-LH surge. Computational modeling is used to manipulate multiple conductances simultaneously and support a role for certain calcium channels in facilitating a switch in firing mode from tonic to bursting. CRISPR knockdown of the TRPC5 channel reduced overall excitability, but this was only examined in cells from ovariectomized mice without estradiol treatment. The patch clamp experiments are comprehensive and overall solid but a direct demonstration of the role of these conductances in being necessary for surge generation (or at least having a direct physiological consequence on surge properties) is lacking, substantially reducing the impact of the findings.*
>
> *Strengths:*

> *(1) Examination of multiple types of calcium and potassium currents, both through electrophysiology and molecular biology.*
>
> *(2) Focus on arcuate kisspeptin neurons during the surge is relatively conceptually novel as the anteroventral periventricular nucleus (AVPV) kisspeptin neurons have received much more attention as the "surge generator" population.*
>
> *(3) The modeling studies allow for direct examination of manipulation of single and multiple conductances, whereas the electrophysiology studies necessarily require examination of each current in isolation. The construction of an arcuate kisspeptin neuron model promises to be of value to the reproductive neuroendocrinology field.*

We thank the reviewer for recognizing our comprehensive examination of Kiss-ARH neurons through electrophysiological, molecular and computational modeling of their activity during the preovulatory surge, which as the reviewer pointed out is “conceptually novel.” We will bolster our argument that Kiss1-ARH neurons transition from synchronized firing to burst firing with the E2-mediated regulation of channel expression with the addition of new experiments. We will address the weaknesses as follows:

> *Weaknesses:*
>
> *(1) The novelty of some of the experiments needs to be clarified. This reviewer's understanding is that prior experiments largely used a different OVX+E2 treatment paradigm mimicking periods of low estradiol levels, whereas the present work used a "high E2" treatment model. However, Figures 10C and D are repeated from a previous publication by the same group, according to the figure legend. Findings from "high" vs. "low" E2 treatment regimens should be labeled and clearly separated in the text. It would also help to have direct comparisons between results from low E2 and high E2 treatment conditions.*

We will revise Figures 10C and 10D to include new findings on Tac2 and Vglut2 expression in OVX and E2-treated Kiss1ARH. We did show the previously published data (Qiu, eLife 2018) to contrast with Figures 10E, F showing the downregulation of TRPC5 and GIRK2 channels following E2 treatment. Most importantly, our E2 treatment regime is clearly stated in the Methods and is exactly the same that was used previously (Qiu, eLife 2016 and Qiu, eLife 2018) for the induction of the LH surge in OVX mice (Bosch, Molecular and Cellular Endocrinology 2013) .

> *(2) In multiple places, links are made between the changes in conductances and the transition from peptidergic to glutamatergic neurotransmission. However, this relationship is never directly assessed. The data that come closest are the qPCR results showing reduced Tac2 and increased Vglut2 mRNA, but in the figure legend, it appears that these results are from a prior publication using a different E2 treatment regimen.*

In the revised Figure 1, we will now include a clear depiction of the transition from synchronized firing driven by NKB signaling in OVX females to burst firing driven by glutamate in E2-treated females. We have used the same E2 treatment paradigm as previously published (Qiu, eLife 2018).

> *(3) Similarly, no recordings of arcuate-AVPV glutamatergic transmission are made so the statements that Kiss1ARH neurons facilitate the GnRH surge via this connection are still only conjecture and not supported by the present experiments.*

Using a horizontal hypothalamic slice preparation, we have shown that Kiss1-ARH neurons excite GnRH neurons via Kiss1ARH glutaminergic input to Kiss1AvPV neurons (summarized in Fig. 12, Qiu, eLife 2016). We do not think that it is necessary to repeat these experiments in the current manuscript.

> *(4) Figure 1 is not described in the Results section and is only tenuously connected to the statement in the introduction in which it is cited. The relevance of panels C and D is not clear. In this regard, much is made of the burst firing pattern that arises after E2 treatment in the model, but this burst firing pattern is not demonstrated directly in the slice electrophysiology examples.*

We will revised Figure 1 to include new whole-cell, current clamp recordings documenting the burst firing in response to glutamate in E2-treated, OVX females.

> *(5) In Figure 3, it would be preferable to see the raw values for R1 and R2 in each cell, to confirm that all cells were starting from a similar baseline. In addition, it is unclear why the data for TTA-P2 is not shown, or how many cells were recorded to provide this finding.*

Before initiating photo-stimulation for each Kiss1-ARH neuron, we adjust the resting membrane potential to -70 mV, as noted in each panel in Figure 3, through current injections. We will include new findings on the effects of the T-channel blocker TTA-P2 on slow EPSP in the revised Figure 3. The number of cells tested with each calcium channel blocker is depicted in each of the bar graphs summarizing the effects of the blockers.

> *(6) In Figure 5, panel C lists 11 cells in the E2 condition but panel E lists data from 37 cells. The reason for this discrepancy is not clear.*

In Figure 5E, we measured the L-, N-, P/Q and R channel currents after pretreatment with TTA-P2 to block the T-type current, whereas in Figure 5C, we measured the current without TTA-P2.

> *(7) In all histogram figures, it would be preferable to have the data for individual cells superimposed on the mean and SEM.*

In all revised Figures we will include the individual data points for the individual neurons.

> *(8) The CRISPR experiments were only performed in OVX mice, substantially limiting interpretation with respect to potential roles for TRPC5 in shaping arcuate kisspeptin neuron function during the preovulatory surge.*

The TRPC5 channels are most important for generating slow EPSPs when expression of NKB is high in the OVX state. Conversely, the glutamatergic response becomes more significant when the expression of NKB and TRPC5 channel are muted. Therefore, the CRISPR experiments were specifically conducted in OVX mice to maximize the effects.

> *(9) Furthermore, there are no demonstrations that the CRISPR manipulations impair or alter the LH surge.*

In this manuscript, our focus is on the cellular electrophysiological activity of the Kiss1ARH neurons in ovx and E2-treated females. Exploration of CRISPR manipulations related to the LH surge is certainly slated for future experiments, but these in vivo experiments are beyond the scope of these comprehensive cellular electrophysiological and molecular studies.

*(10) The time of day of slice preparation and recording needs to be specified in the Methods.*

We will provide the times of slice preparation and recordings in the revised Methods and Materials.

***Reviewer #2 (Public Review):***

*Summary:*

*Kisspeptin neurons of the arcuate nucleus (ARC) are thought to be responsible for the pulsatile GnRH secretory pattern and to mediate feedback regulation of GnRH secretion by estradiol (E2). Evidence in the literature, including the work of the authors, indicates that ARC kisspeptin coordinate their activity through reciprocal synaptic interactions and the release of glutamate and of neuropeptide neurokinin B (NKB), which they co-express. The authors show here that E2 regulates the expression of genes encoding different voltage-dependent calcium channels, calcium-dependent potassium channels, and canonical transient receptor potential (TRPC5) channels and of the corresponding ionic currents in ARC kisspeptin neurons. Using computer simulations of the electrical activity of ARC kisspeptin neurons, the authors also provide evidence of what these changes translate into in terms of these cells' firing patterns. The experiments reveal that E2 upregulates various voltage-gated calcium currents as well as 2 subtypes of calcium-dependent potassium currents while decreasing TRPC5 expression (an ion channel downstream of NKB receptor activation), the slow excitatory synaptic potentials (slow EPSP) elicited in ARC kisspeptin neurons by NKB release and expression of the G protein-associated inward-rectifying potassium channel (GIRK). Based on these results, and on those of computer simulations, the authors propose that E2 promotes a functional transition of ARC kisspeptin neurons from neuropeptide-mediated sustained firing that supports coordinated activity for pulsatile GnRH secretion to a less intense firing in glutamatergic burst-like firing pattern that could favor glutamate release from ARC kisspeptin. The authors suggest that the latter might be important for the generation of the preovulatory surge in females.*

*Strengths:*

*The authors combined multiple approaches in vitro and in silico to gain insights into the impact of E2 on the electrical activity of ARC kisspeptin neurons. These include patch-clamp electrophysiology combined with selective optogenetic stimulation of ARC kisspeptin neurons, reverse transcriptase quantitative PCR, pharmacology, and CRIPR-Cas9-mediated knockdown of the Trpc5 gene. The addition of computer simulations for understanding the impact of E2 on the electrical activity of ARC kisspeptin cells is also a strength.*

*The authors add interesting information on the complement of ionic currents in ARC kisspeptin neurons and on their regulation by E2 to what was already known in the literature. Pharmacological and electrophysiological experiments appear of the highest standards. Robust statistical analyses are provided throughout, although some experiments (illustrated in Figures 7 and 8) do have rather low sample numbers.*

*The impact of E2 on calcium and potassium currents is compelling. Likewise, the results of Trpc5 gene knockdown do provide good evidence that the TRPC5 channel plays a key role in mediating the NKB-mediated slow EPSP. Surprisingly, this also revealed an unsuspected role for this channel in regulating the membrane potential and excitability of ARC kisspeptin neurons.*

We thank the reviewer for recognizing that the “pharmacological and electrophysiological experiments appear of the highest standards” and “the addition of the computer modeling for understanding the impact of E2 on the electrical activity of ARC kisspeptin cells is also a strength. However, we agree with the reviewer that we need to provide a direct demonstration of “burst-like” firing of Kiss1-ARH neurons. We will address the weaknesses as follows:

> *Weaknesses:*
>
> *The manuscript also has weaknesses that obscure some of the conclusions drawn by the authors.*
>
> *One has to do with the fact that "burst-like" firing that the authors postulate ARC kisspeptin neurons transition to after E2 replacement is only seen in computer simulations, and not in slice patch-clamp recordings. A more direct demonstration of the existence of this firing pattern, and of its prominence over neuropeptide-dependent sustained firing under conditions of high E2 would make a more convincing case for the authors' hypothesis.*

We will provide a more direct demonstration of the existence of this firing pattern in the whole-cell current clamp experiments in the revised Figure 1.

> *In addition, and quite importantly, the authors compare here two conditions, OVX versus OVX replaced with high E2, that may not reflect the physiological conditions (the diestrous [low E2] and proestrous [high E2] stages of the estrous cycle) under which the proposed transition between neuropeptide-dependent sustained firing and less intense burst firing might take place. This is an important caveat to keep in mind when interpreting the authors' findings. Indeed, that E2 alters certain ionic currents when added back to OVX females, does not mean that the magnitude of these ionic currents will vary during the estrous cycle.*

We have published that the magnitude of the slow EPSP, which is TRPC5 channel mediated, varies throughout the estrous cycle and the similarity to that found in OVX compared to E2-treated, OVX females (Figure 2, Qiu, eLife 2016). Moreover, TRPC5 channel mRNA expression, similar to the peptides, is downregulated by an E2 treatment (Figure 10 this manuscript) that mimics proestrus levels of the steroid (Bosch, Mol Cell Endocrinology 2013). Furthermore, the magnitude of ionic currents is directly proportional to the number of ion channels expressed in the plasma membrane, which we have found correlates with mRNA expression. Therefore, it is likely that the magnitude of these ionic currents will vary during the estrous cycle.

> *Lastly, the results of some of the pharmacological and genetic experiments may be difficult to interpret as presented. For example, in Figure 3, although it is possible that blockade of individual calcium channel subtypes suppresses the slow EPSP through decreased calcium entry at the somato-dendritic compartment to sustain TRPC5 activation and the slow depolarization (as the authors imply), a reasonable alternative interpretation would be that at least some of the effects on the amplitude of the slow EPSP result from suppression of presynaptic calcium influx and, thus, decreased neurotransmitter and neuropeptide secretion. Along the same lines, in Figure 12, one possible interpretation of the observed smaller slow EPSPs seen in mice with mutant TRPC5 could be that at least some of the effect is due to decreased neurotransmitter and neuropeptide release due to the decreased excitability associated with TRPC5 knockdown.*

The reviewer raises a good point, but our previous findings clearly demonstrate that chelating intracellular calcium with BAPTA in whole-cell current clamp recordings abolishes the slow EPSP and persistent firing (Qiu, J. Neurosci 2021), which we have noted is the rationale for dissecting out the contribution of T, R, N, L and P/Q calcium channels to the slow EPSP in our current studies (revised Figure 3 will include the effects of T-channel blocker).

However, to further bolster the argument for the post-synaptic contribution of the calcium channels to the slow EPSP and eliminate the potential presynaptic effects of calcium channel blockers on the postsynaptic slow EPSP amplitude, which may result from reduced presynaptic calcium influx and subsequently decreased neurotransmitter release, we will utilized an additional strategy. Specifically, we will measure the response to the externally administered TACR3 agonist senktide under conditions in which the extracellular calcium influx, as well as neurotransmitter and neuropeptide release, are blocked (new Figure 3).